

# RESONANCE BROADENING AND HEATING OF CHARGED PARTICLES IN MAGNETOHYDRODYNAMIC TURBULENCE

JACOB W. LYNN<sup>1,2</sup>, IAN J. PARRISH<sup>2</sup>, ELIOT QUATAERT<sup>2</sup>, & BENJAMIN D. G. CHANDRAN<sup>3</sup>

*Draft version August 15, 2018*

## ABSTRACT

The heating, acceleration, and pitch-angle scattering of charged particles by MHD turbulence are important in a wide range of astrophysical environments, including the solar wind, accreting black holes, and galaxy clusters. We simulate the interaction of high-gyrofrequency test particles with fully dynamical simulations of subsonic MHD turbulence, focusing on the parameter regime with  $\beta \sim 1$ , where  $\beta$  is the ratio of gas to magnetic pressure. We use the simulation results to calibrate analytical expressions for test particle velocity-space diffusion coefficients and provide simple fits that can be used in other work.

The test particle velocity diffusion in our simulations is due to a combination of two processes: interactions between particles and magnetic compressions in the turbulence (as in linear transit-time damping; TTD) and what we refer to as Fermi Type-B (FTB) interactions, in which charged particles moving on field lines may be thought of as beads sliding along moving wires. We show that test particle heating rates are consistent with a TTD resonance which is broadened according to a decorrelation prescription that is Gaussian in time (but inconsistent with Lorentzian broadening due to an exponential decorrelation function, a prescription widely used in the literature). TTD dominates the heating for  $v_s \gg v_A$  (e.g. electrons), where  $v_s$  is the thermal speed of species  $s$  and  $v_A$  is the Alfvén speed, while FTB dominates for  $v_s \ll v_A$  (e.g. minor ions). Proton heating rates for  $\beta \sim 1$  are comparable to the turbulent cascade rate. Finally, we show that velocity diffusion of collisionless, large gyrofrequency particles due to large-scale MHD turbulence does not produce a power-law distribution function.

## 1. INTRODUCTION

The interaction between charged particles and magnetohydrodynamic (MHD) turbulence plays a role in the energy balance of diverse astrophysical environments such as the solar corona and solar wind (e.g. Cranmer et al. 2007) and accretion disks around black holes (e.g. Quataert & Gruzinov 1999). The coupling between turbulence and particles is also important for the transport and confinement of cosmic rays in galaxies (e.g. Chandran 2000; Yan & Lazarian 2004).

This paper focuses on the interaction of test particles with subsonic (and thus weakly compressible) MHD turbulence. Such turbulence consists primarily of nonlinearly interacting Alfvén waves which drive the turbulent cascade (Kraichnan 1965; Shebalin et al. 1983; Goldreich & Sridhar 1995), along with slow magnetosonic modes that are advected passively by the Alfvénic cascade (Lithwick & Goldreich 2001; Cho & Lazarian 2002). On observational (Chen et al. 2011), theoretical (Goldreich & Sridhar 1995), and numerical (Maron & Goldreich 2001; Beresnyak 2011) grounds, the MHD cascade is believed to be strongly anisotropic, with most power in the inertial range of the cascade in modes with wavevectors primarily perpendicular to the magnetic field. This has many implications for the coupling between particles and turbulence, including e.g. that cyclotron heating of

particles by the MHD cascade is significantly suppressed (Quataert 1998; Cranmer & van Ballegoijen 2003, though see Leamon et al. (1999); Gary & Borovsky (2008); Jiang et al. (2009) for discussions of the cyclotron resonance in the corona and solar wind).

The interaction between test particles and plasma waves has been extensively studied in the “quasilinear” approximation (Kennel & Engelmann 1966; Jokipii 1966), which stipulates that test particles execute unperturbed helical motion around magnetic field lines, and that plasma waves are long-lived relative to their periods. This implies that wave-particle interactions and energy exchange occur only at discrete resonances (Stix 1992, and references therein). To the extent that MHD turbulence is well-described by a superposition of long-lived small-amplitude plasma waves, quasilinear theory will accurately describe test particle diffusion and heating in turbulence.

However, the picture of strong anisotropic MHD turbulence developed over the last  $\sim 30$  years by many authors (e.g. Montgomery & Turner 1981; Shebalin et al. 1983; Higdon 1984; Goldreich & Sridhar 1995, henceforth GS) suggests that the Alfvén and slow waves comprising weakly compressible MHD turbulence are not long-lived, and instead decorrelate due to non-linear interactions before they can propagate over distances of multiple wavelengths.<sup>4</sup> As a result, the discrete resonances of quasilinear theory are expected to be substantially broadened in MHD turbulence (e.g. Bieber et al.

<sup>1</sup> Physics Department, University of California, Berkeley, CA 94720; jacob.lynn@berkeley.edu

<sup>2</sup> Astronomy Department and Theoretical Astrophysics Center, University of California, Berkeley, CA 94720

<sup>3</sup> Space Science Center and Department of Physics, University of New Hampshire, Durham, NH 03824

<sup>4</sup> The use of *strong* here refers to this state of “critical balance” between eddy and wave timescales, rather than the amplitude of the turbulence.

1994; Shalchi et al. 2004; Shalchi & Schlickeiser 2004; Qin et al. 2006; Yan & Lazarian 2008).

In this paper, we study the interaction between test particles and driven MHD turbulence (see also earlier work by Dmitruk et al. 2004; Lehe et al. 2009). In particular, we quantify the velocity-space diffusion, particle heating, and particle acceleration that results. We compare these numerical results in detail to analytic models and, in particular, calibrate models of resonance broadening. Our focus is on the basic physics—the diffusion coefficients we calculate (e.g. eqn. 10 & 13 & Table 2) can be used for a wide range of applications, some of which we will explore in detail in future studies.

The paper is structured as follows. In §2, we summarize the qualitative features of test particle interactions with turbulence, including both resonance broadening and non-resonant interactions. In §3 we use these physical ideas to derive analytical expressions for velocity diffusion coefficients in turbulence, while in §4 we calculate the resulting heating rates for a thermal distribution of test particles. Many of these results are not new, but they provide a useful analytic framework for interpreting our test particle numerical results and so are included for completeness. In §5 we describe our numerical methods for evolving test particles in simulations of MHD turbulence, and in §6 we compare our analytical predictions to the results of test particle simulations. Finally, in §7 we discuss the conclusions and implications of our work. We also include several Appendices which consider related ideas. In Appendix A, we discuss the interaction of test particles with one finite-amplitude wave, in Appendix B, we consider an extension of our model into a regime of weak turbulence, and in Appendix C, we discuss the power spectra of our turbulence simulations in the context of weak and strong turbulence.

## 2. QUALITATIVE DISCUSSION OF TEST PARTICLE TRANSPORT IN MHD TURBULENCE

In this paper, we focus on isothermal MHD turbulence with  $\beta = \rho c_s^2 / (B_0^2 / 8\pi) \sim 1$  and  $\epsilon$  such that the turbulence is subsonic and sub-Alfvénic, where  $\epsilon$  is the energy input rate per unit mass into the turbulence. Additionally, we focus on high-gyrofrequency particles with  $\Omega \gg \omega_{\max}$ , where  $\Omega = qB/mc$  is the particle cyclotron frequency and  $\omega_{\max}$  is the maximum resolveable wave frequency in the turbulence. Our motivation for doing so is that this inequality is believed to be satisfied even deep in the inertial range of weakly compressible MHD turbulence (see e.g. Howes et al. 2008). In addition to  $\Omega \gg \omega_{\max}$ , magnetic moment conservation generally also requires that the amplitude of the turbulent fluctuations on scales of the Larmor radius  $r_L$  satisfy  $\delta v / v_\perp \ll 1$  (McChesney et al. 1987; Chaston 2004; Chandran et al. 2010). This is satisfied in our simulations both because we focus on subsonic  $\beta \sim 1$  turbulence and because the Kolmogorov power spectrum that the turbulence self-consistently develops has only modest power on small scales  $\sim r_L$ . We shall see that magnetic moment conservation is indeed reasonably well satisfied in our test particle simulations (see §6). This implies that particle acceleration will be primarily in the parallel direction. (We use the subscripts  $\parallel$  and  $\perp$  throughout to indicate parallel and perpendicular to the local magnetic field, respectively.)

Generically, there will be two processes that cause changes in parallel velocity for the high- $\Omega$  particles under consideration. The first is *transit-time damping* (TTD), which is analogous to Landau damping. In a spatially-varying magnetic field, charged particles feel mirror forces, given by  $\mu \nabla_\parallel B$ , where  $\mu = mv_\perp^2 / 2B$  is the particle’s magnetic moment. If the spatial variation is provided by a compressive wave moving with a phase speed  $v_p$ , then particles with  $v_\parallel \simeq v_p$  will “surf” the wave and experience correlated acceleration for long times (until the particle is accelerated such that it is no longer in resonance). On the other hand, a particle with  $v_\parallel \neq v_p$  will experience time-varying accelerations that will average to zero over long times. Thus, over time scales sufficiently short that particle velocities do not change substantially (where linear theory applies) the interaction of the wave with a distribution of particles will be given by a delta-function,  $D_\parallel \propto \delta(v_\parallel - v_p)$ , where  $D_\parallel$  is the parallel velocity diffusion coefficient.

This picture will be modified for the interaction of particles with strong turbulence. Strong turbulence can be thought of as a distribution of waves, which nonetheless do not propagate long distances as waves, but instead decohere on a timescale  $\omega^{-1}$ , where  $\omega$  is the frequency of the wave. The linear theory model for the interaction of particles and waves is only valid for waves that are relatively long-lived; qualitatively, wave decoherence will cause the delta-function resonance to broaden, with more particles able to approximately satisfy the resonance condition for long enough to experience significant acceleration.

Because TTD arises from the mirror force, it will become negligible as  $\mu \rightarrow 0$ . In this limit (and in the high- $v_\parallel$  limit, as we will show) the most important mechanism for changes in parallel velocity is what we refer to as *Fermi Type-B* (FTB) acceleration (Fermi 1949). Consider a particle spiralling along a magnetic field line with some curvature (see Fig. 1). In the frame of the field line, the particle has constant energy, because magnetic fields do no work. In the frame of the bulk plasma (i.e., the frame in which the average fluid momentum is zero), however, the particle may gain or lose energy. This can be seen straightforwardly with a Galilean transform (in the non-relativistic case) from the field line frame to the plasma frame. Qualitatively, FTB describes charged particles as beads sliding along moving wires. These stochastic interactions will also cause diffusion in velocity space independent of  $\mu$ .

As noted above, we do not consider particles with  $\Omega \sim \omega$ . Particles with  $\omega - k_\parallel v_\parallel = n\Omega$ , where  $n$  is a non-zero integer, are “cyclotron-resonant” and can thus experience violation of  $\mu$ -conservation and strong perpendicular heating. However, due to the anisotropy of the strong MHD turbulent cascade (Goldreich & Sridhar 1995), MHD turbulence with a substantial inertial range may transfer its energy into a kinetic Alfvén wave cascade on scales of  $k_{\perp, \max} \sim r_L^{-1}$ , where  $r_L$  is the proton gyroradius. At this scale in the solar wind, the maximum gyrofrequency that can be cyclotron-resonant for thermal particles is  $\ll \Omega_p$ , the proton gyrofrequency (see Lehe et al. 2009). As a result, any cyclotron heating of protons or electrons occurs (if it occurs at all) on scales below the MHD cascade that we consider here. However, there is recent work (Cranmer & van Ballegoijen 2012)

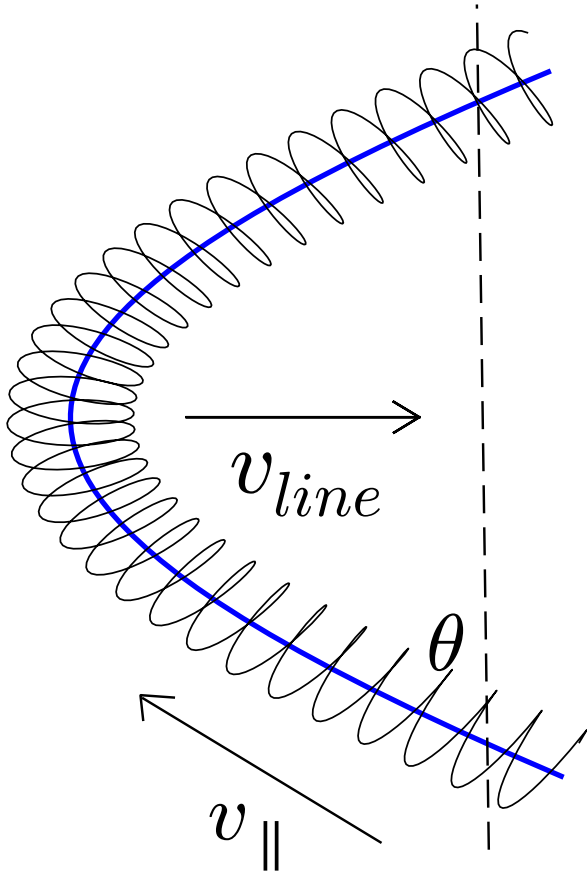


FIG. 1.— In a Fermi Type-B interaction, a particle moving with parallel velocity  $v_{\parallel}$  along a curved element of magnetic field line will gain or lose parallel velocity  $\Delta v_{\parallel} = v_{\text{line}} \sin \theta$ , assuming the pictured geometry, due to being slung around like a “bead on a wire.”

suggesting that mode coupling between the isotropic fast mode cascade and Alfvén modes could supply enough high- $k_{\parallel}$  power in the solar wind to heat protons through the cyclotron resonance.

Our test particle calculations presented in §3 do not include diffusion due to parallel electric fields (Landau damping). The reason is that our simulations are performed in the ideal MHD limit. Physically, sound waves in a collisionless plasma do generate significant parallel electric fields – this effect is potentially important for the fast mode in  $\beta \gtrsim 1$  MHD turbulence and for the slow mode in  $\beta \lesssim 1$  turbulence, but is not captured in our test particle calculations. Additionally, the ideal MHD limit does not allow us to capture heating and acceleration by magnetic reconnection, which is likely an important mechanism in many astrophysical environments including solar flares (see e.g. Drake et al. 2006, 2009).

### 3. ANALYTIC TRANSPORT PROPERTIES

In this section, we provide an analytic derivation of the evolution of a distribution of test particles in velocity space as they interact with Alfvénic MHD turbulence. We focus on the diffusive evolution in  $v_{\parallel}$ , which dominates over any changes in  $v_{\perp}$ , as argued in §2.

#### 3.1. Transport in $v_{\perp}$

The magnetic moment  $\mu = v_{\perp}^2/B$  is approximately a conserved quantity in our test particle calculations described in §5 (for more discussion, see §2).

If  $\mu$  is conserved, then any change in  $v_{\perp}$  results from a change in the local value of the magnetic field. A distribution of particles that initially all have the same value of  $v_{\perp}$ , randomly initialized in space throughout a turbulent plasma, will quickly broaden in  $v_{\perp}$  over short time scales, and then reach a saturated width in  $v_{\perp}$  as the particles statistically sample all of the fluctuations in  $B$ . Taking a differential of  $v_{\perp} = \sqrt{\mu B}$ , we find that final width of the distribution in  $v_{\perp}$  will be approximately given by  $\delta v_{\perp}/v_{\perp} \sim B_L/2B_0$ , where  $B_L$  is the rms deviation of  $B$  from the mean. We can understand this more simply by noting that if a particle is initialized where  $B$  is higher than  $B_0$ , then  $\mu$  for that particle will be lower than the average. Thus the fractional width of the initial distribution in  $\mu$  will be the same as the width of the initial distribution in  $B$  (in the  $B_L/B_0 \ll 1$  limit). After some time passes and the test particles statistically sample the turbulence, a particle with a smaller  $\mu$  is not preferentially likely to be in a location of larger magnetic field, so this particle will have a smaller time-averaged  $v_{\perp}$ . To the extent that  $\mu$  is well-conserved, there will be little diffusion in  $v_{\perp}$  after this initial re-adjustment.

#### 3.2. Transport in $v_{\parallel}$

Diffusion in parallel velocity in our simulations comes from two sources, which Fermi (1949) referred to as “Type A” and “Type B” interactions. Type A refers to acceleration by magnetic mirror forces. In Fermi’s original conception, charged particles reflected off of magnetic inhomogeneities (clouds) due to the  $\mu \nabla B$  force. In this work, the scattering centers are compressive MHD modes, so that Type A acceleration and TTD are effectively the same. Type B refers to the acceleration of a particle in the rest frame of the bulk plasma, due to following a curved, moving field line.

##### 3.2.1. TTD and Resonance Broadening

A particle moving in compressible MHD turbulence will be randomly accelerated and decelerated by mirror forces, given by  $\mu \nabla B$ . This will lead to diffusion in parallel velocity given by

$$\frac{\partial f}{\partial t} = \frac{\partial}{\partial v_{\parallel}} \left( D_{\parallel} \frac{\partial f}{\partial v_{\parallel}} \right), \quad (1)$$

where  $f(\mathbf{x}, \mathbf{v})$  is the velocity-space distribution function (we will assume a uniform spatial distribution of test particles throughout). We adopt the formal approach of Dupree (1966) and Weinstock (1969) and write the corresponding diffusion coefficient as

$$D_{\parallel} = \mu^2 \int_0^{\infty} dt \langle \nabla_{\parallel} B(\mathbf{r}_0, 0) \nabla_{\parallel} B(\mathbf{r}(t), t) \rangle, \quad (2)$$

where  $\langle \rangle$  indicates an ensemble average,  $\nabla_{\parallel}$  means the gradient in the parallel (to the magnetic field) direction, and  $\mathbf{r}(t)$  describes a particle’s trajectory. Introducing a Fourier transform of the magnetic field, we can then

write Equation 2 as

$$D_{\parallel} = \frac{\mu^2}{(2\pi)^3} \int d^3k k_{\parallel}^2 I(\mathbf{k}) R(\mathbf{k}), \quad (3)$$

where  $I(\mathbf{k})$  is the power spectrum of magnetic field fluctuations, and  $R(\mathbf{k})$  is a resonance function. If we consider only free-streaming trajectories (ignoring any variations in  $v_{\parallel}$ ), as in linear theory, the resonance function is given by

$$R(\mathbf{k}) = \text{Re} \int_0^{\infty} dt e^{i(\omega(\mathbf{k}) - v_{\parallel} k_{\parallel})t}. \quad (4)$$

This resonance function becomes the standard  $\delta(v_{\parallel} \pm v_p)$  for interactions with waves satisfying the linear dispersion relation  $\omega(\mathbf{k}) = \pm |k_{\parallel}| v_p$ . The  $\mu \nabla_{\parallel} B$  force requires compressive fluctuations, and thus will stem from slow or fast waves in MHD turbulence, rather than Alfvén waves. However, the slow mode cascade passively adopts the anisotropic GS power spectrum, with  $k_{\perp} \gg k_{\parallel}$  in the inertial range (Cho & Lazarian 2002). In this regime, the slow mode dispersion relation becomes  $\omega = k_{\parallel} c_s v_A / \sqrt{c_s^2 + v_A^2}$  (Chandran 2003), limiting to  $\omega = k_{\parallel} v_A$  for  $\beta \gg 1$  and  $\omega = k_{\parallel} c_s$  for  $\beta \ll 1$ . For analytical simplicity, we use a generic Alfvénic dispersion relation,  $\omega = k_{\parallel} v_p$ , where  $v_p$  is the appropriate phase velocity. The specification of the results presented here to various slow mode regimes is straightforward.

Deviation from free-streaming trajectories modifies the resonance function in Equation 4 (Weinstock 1969); the resonance function becomes

$$R(\mathbf{k}) = \text{Re} \int_0^{\infty} dt e^{i(\omega(\mathbf{k}) - v_{\parallel} k_{\parallel})t + \frac{1}{2} \langle [i\mathbf{k} \cdot \delta\mathbf{r}(t)]^2 \rangle}, \quad (5)$$

where  $\delta\mathbf{r}(t)$  describes the deviation of a particle’s trajectory, and we have assumed the mean deviation  $\langle \delta\mathbf{r}(t) \rangle = 0$ . Formally, this result requires  $k\tau_B^2 \mu \nabla_{\parallel} B \ll 1$ , where  $\tau_B$  is the correlation time of the stochastic magnetic field fluctuations on a given scale  $k$ , which will not hold for all scales or for all test particles we consider. Furthermore, the exact value of  $\langle [\delta\mathbf{r}(t)]^2 \rangle$  depends on the diffusion coefficient that we are trying to calculate, and would require a recursive approach to calculating  $D_{\parallel}$  and  $D_{\perp}$ . Thus, for analytical simplicity, we use Equation 5 only to motivate a phenomenological modification to the resonance function.

To estimate an appropriate modification, consider that one source of deviation from free-streaming trajectories is the fact that high- $\mu$  particles are tied to magnetic field lines that can wander in the perpendicular direction. This process will be essentially stochastic and therefore diffusive. The typical step length will be given by  $v_l \tau_B$ , where  $v_l$  is the scale-dependent rms turbulent velocity. Thus:

$$\langle \delta\mathbf{r}_{\perp}^2(t) \rangle \sim (v_l \tau_B)^2 \left( \frac{t}{\tau_B} \right) \sim v_l^2 \tau_B t. \quad (6)$$

Throughout the main body of the paper we focus on the strong anisotropic turbulence model of Goldreich & Sridhar (1995, henceforth GS), though we consider an extension to weak turbulence in Appendix B.<sup>5</sup> In the GS model, the correlation time of fluctuations is given by  $\tau_B^{-1} \sim \omega_{\text{nl}} = (k_{\perp} L)^{2/3} v_L / L$ , where  $v_L$  is

<sup>5</sup> Note that since we drive our test particle simulations in §6

the rms turbulent velocity on the driving scale  $L$ . This timescale may be thought of as the “lifetime” of waves in turbulence. Thus our estimate for the field line random-walk deviation becomes

$$\langle [\mathbf{k} \cdot \delta\mathbf{r}(t)]^2 \rangle \sim v_L (k_{\perp} L)^{2/3} t / L = \omega_{\text{nl}} t. \quad (7)$$

The equality above suggests that we could have reached the same conclusion via the somewhat different approach of directly modifying the time dependence of the wave modes in our turbulence:  $e^{i\omega t} \rightarrow e^{i\omega t - \omega_{\text{nl}} t}$  (defined for  $t > 0$ ). This alternative approach directly describes the modes themselves as decohering on a timescale  $\omega_{\text{nl}}^{-1}$ . We will refer to this as the *exponential decorrelation* model.

To account for the uncertainty in these estimates, we replace the factor of 1/2 in Equation 5 with  $\gamma$ , a dimensionless order-unity constant. In this section we also choose to instead use  $\omega_{\text{nl}} = (2\pi v_A / L) (k_{\perp} L / 2\pi)^{2/3}$ , the generic “strong turbulence” expression for the non-linear turnover time.<sup>6</sup> This is for the sake of generality: for MHD turbulence with a significant inertial range, even if the turbulence is weak on the outer scales, the nonlinearity of the turbulence increases on smaller scales, eventually approaching critical balance. When critical balance is reached, the remainder of the cascade will be in the strong regime. Furthermore, the turbulence is weak on the outer scales, where the turbulence is being driven. Thus, the details of the driving are more likely to be important for the turbulence statistics in the weak regime. We present analytic calculations of resonance broadening in weak turbulence in Appendix B.

Given Equation 7, we can perform the integral in Equation 5 to calculate the exponential resonance function,

$$R_{\text{exp}}(\mathbf{k}) = \frac{\gamma v_A (k_{\perp} L)^{2/3} (2\pi)^{1/3}}{\gamma^2 v_A^2 (2\pi)^{2/3} (k_{\perp} L)^{4/3} / L + k_{\parallel}^2 L (v_{\parallel} \pm v_p)^2}, \quad (8)$$

where we have used the dispersion relation,  $\omega(\mathbf{k}) = \pm v_p |k_{\parallel}|$ . We see that the resonance function is still peaked at  $|v_{\parallel}| = v_p$ , but becomes a Lorentzian in  $v_{\parallel}$  rather than a delta-function.

To calculate the parallel diffusion coefficient  $D_{\parallel}$  associated with this broadened resonance, we perform the integral in Equation 3, using a power spectrum of the GS form,

$$I(\mathbf{k}) \propto v_L^2 k_{\perp}^{-10/3} g\left(\frac{k_{\parallel} L^{1/3}}{k_{\perp}^{2/3}}\right), \quad (9)$$

normalized such that  $v_L^2 / 2 = \int d^3\mathbf{k} I(\mathbf{k}) / (2\pi)^3$ . In this expression, we will treat  $g(x)$  as a step function, equal to 1 if  $|x| < 1$ , and 0 otherwise, which accounts for the fact that power only resides in  $k_{\parallel} \ll k_{\perp}$  in the iner-

at sub-Alfvénic velocities on the outer scale, we are in fact in the weak/intermediate turbulence regime on size scales of  $l_{\perp} \gtrsim l_c \equiv LM_A^2$ , where  $L$  is the outer (driving) scale of the turbulence and  $M_A$  refers to the Alfvénic Mach number at  $L$  (see e.g. Goldreich & Sridhar 1997; Galtier et al. 2000). We discuss an extension of the model in this section which incorporates weak turbulence in Appendix B.

<sup>6</sup> If one considers a simulation with fixed  $k$  and  $v_A$  (i.e., a fixed simulation box), decreasing  $\dot{\epsilon}$  (and therefore  $v_L$ ) corresponds to weaker turbulence, since  $\omega_{\text{nl}} < \omega \sim k_{\parallel} v_A$ .

tial range of the cascade.<sup>7</sup> The turbulence model described here is broadly supported by numerical simulations (Maron & Goldreich 2001; Cho & Lazarian 2002; Beresnyak 2012). However, it is not universally accepted; see Boldyrev (2006), Perez & Boldyrev (2008), and Grappin & Müller (2010) for discussions of possible shortcomings of this model. Substituting Equation 9 into Equation 3 and performing the integral leads to

$$D_{\parallel} \equiv C_1 G v_{\perp}^4 \left[ \frac{1}{u_{-}^2} \left( 1 - \frac{1}{u_{-}} \arctan u_{-} \right) + \frac{1}{u_{+}^2} \left( 1 - \frac{1}{u_{+}} \arctan u_{+} \right) \right], \quad (10)$$

where  $u_{\pm} = (v_{\parallel} \pm v_p)/\gamma v_A$ ,  $C_1$  is a dimensionless constant,  $G \equiv v_L^2 \pi \log(L/L_{\min})/(6 \gamma L v_A^3)$  is a function which absorbs normalization constants, and  $L_{\min}$  is the smallest resolvable length scale on the grid. We leave the normalization constant  $C_1$  unspecified at the moment; if our previous calculations were exact, then  $C_1$  would be equal to 1. We will calibrate this value against our test particle simulations in §6. Equation 10 has the limiting values

$$D_{\parallel} \propto \begin{cases} \text{const} & \text{if } |v_{\parallel}| \ll v_p \\ v_p^2/v_{\parallel}^2 & \text{if } |v_{\parallel}| \gg v_p. \end{cases} \quad (11)$$

Again, we see that the delta-function resonance predicted by linear theory is substantially broadened, so that all particles with  $|v_{\parallel}| \lesssim v_A$  couple equally well to the turbulence; in addition, high-velocity particles can also interact with the turbulence via the TTD resonance.

It is not entirely clear on theoretical grounds that the exponential decorrelation of the preceding discussion is the correct or the only model for resonance broadening. Thus we consider also a simple alternative, which we refer to as a *Gaussian decorrelation* model. We replace  $e^{-\gamma \omega_{\text{nl}} t}$  in Equation 9 with  $e^{-(\gamma \omega_{\text{nl}} t)^2}$ , where  $\gamma$  has qualitatively the same physical interpretation as in the exponential case. We argue that this functional form for the wave decoherence is more physically motivated as it has smooth derivatives as  $t \rightarrow 0$ . In this case, we find the Gaussian resonance function,

$$R_{\text{gauss}}(\mathbf{k}) = \frac{\pi^{1/6} L}{\gamma v_A (4k_{\perp} L)^{2/3}} \times \exp \left[ -\frac{k_{\parallel}^2 L^2 (v_{\parallel} \pm v_p)^2}{4\gamma^2 v_A^2 (2\pi)^{2/3} (k_{\perp} L)^{4/3}} \right], \quad (12)$$

so that the  $\delta$ -function becomes a Gaussian resonance. Again we use Equation 3 to find

$$D_{\parallel} \equiv C_2 G v_{\perp}^4 \left\{ \frac{1}{u_{-}^3} \left[ \pi \operatorname{erf} \left( \frac{u_{-}}{2} \right) - u_{-} \sqrt{\pi} \exp \left( -\frac{u_{-}^2}{4} \right) \right] + \frac{1}{u_{+}^3} \left[ \pi \operatorname{erf} \left( \frac{u_{+}}{2} \right) - u_{+} \sqrt{\pi} \exp \left( -\frac{u_{+}^2}{4} \right) \right] \right\} \quad (13)$$

<sup>7</sup> The step function approximation for  $g(x)$  is for analytic convenience. Physically, the cutoff in power in the  $k_{\parallel}$  direction is unlikely to be quite so sharp. We have confirmed using numerical calculations that a cutoff in  $k_{\parallel}$  that is, e.g., exponential, rather than a step function, produces quantitatively similar results for the diffusion coefficients of interest.

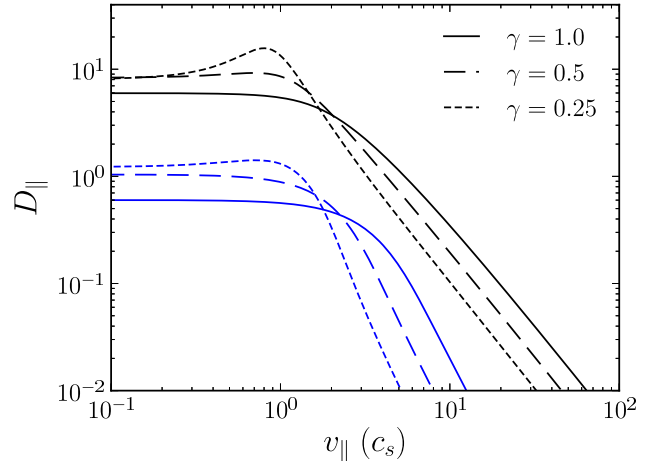


FIG. 2.— Analytic models of the effects of resonance broadening on the parallel velocity diffusion produced by the interaction between particles and strong MHD turbulence. We show both exponential (black lines) and Gaussian (blue) models of resonance broadening (see §3.2.1), with different values of  $\gamma$  indicated by linestyles. Both are arbitrarily normalized, with the exponential models artificially normalized to a higher value for clarity.  $v_p = 0.81 c_s$  is chosen, consistent with  $\beta = 1$  slow modes. The dimensionless parameter  $\gamma$  controls the magnitude of the broadening with  $\gamma \ll 1$  approaching the linear theory prediction of a delta function at  $v_{\parallel} = v_p$ . The exponential resonance function gives  $D_{\parallel} \propto v_{\parallel}^{-2}$  in the high- $v_{\parallel}$  regime, while the Gaussian model gives  $D_{\parallel} \propto v_{\parallel}^{-3}$ .

where  $\operatorname{erf}(x)$  is the error function and  $C_2$  is again a dimensionless normalization constant to be calibrated. This has the limiting values

$$D_{\parallel} \propto \begin{cases} \text{const} & \text{if } |v_{\parallel}| \ll v_p \\ v_p^3/|v_{\parallel}|^3 & \text{if } |v_{\parallel}| \gg v_p. \end{cases} \quad (14)$$

In Figure 2 we plot several representative examples of  $D_{\parallel}$  with arbitrary normalization. The dimensionless parameter  $\gamma$  controls the “peakiness” of the resonance. Note that in all cases  $D_{\parallel}$  declines steeply above  $v_p$ , which implies that TTD heating of very fast particles is inefficient. TTD acts primarily on particles in the bulk of the plasma, near the (linear) resonance.

For completeness, we also calculate the diffusion coefficient resulting from the linear theory delta-function resonance, with  $\omega_{\text{nl}} = 0$ . In this case, the resonance function becomes

$$R(\mathbf{k}) = \frac{\pi}{|k_{\parallel}|} \delta(v_{\parallel} \pm v_p). \quad (15)$$

Once again, we apply the GS power spectrum to the resonant diffusion coefficient of Equation 3 to find

$$D_{\parallel} = \frac{\pi^2}{24L} \left( \frac{v_L}{v_A} \right)^2 v_{\perp}^4 \log \left( \frac{L}{L_{\min}} \right) \delta(v_{\parallel} \pm v_p). \quad (16)$$

### 3.2.2. Resonance broadening of other modes

Our discussion up to this point has focused on slow modes with  $\beta > 1$  for the sake of analytical simplicity. These results are, however, relatively easy to generalize, and can be applied to other wave modes and plasma parameter regimes. For example, analytically accounting for fast modes is not difficult. In Figure 3, we plot

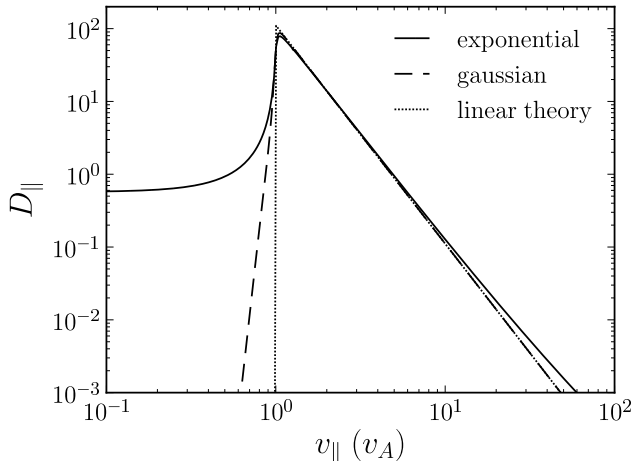


FIG. 3.— Fast mode contribution to resonance-broadened TTD assuming either an exponential or Gaussian form for the decorrelation (arbitrary normalization, with  $\gamma = 1$ ; see §3.2.2 for more details on the calculation). For comparison, we include also fast mode TTD with a delta-function resonance. The weak non-linearity of fast modes in MHD turbulence leads to a sharp resonance, very close to the linear theory result.

numerically-calculated resonance-broadened TTD coefficients associated with fast modes in  $\beta < 1$  turbulence. We include for comparison the diffusion coefficient predicted by a linear theory delta function resonance. (The linear theory diffusion coefficient in this case is not itself a delta-function due to the fast mode resonance condition,  $kv_A = k_{\parallel}v_{\parallel}$ .) Several modifications to the derivation in 3.2.1 are required for the resonance-broadening calculation. We use the fast mode dispersion relation,  $\omega = v_A k$ , and we assume an isotropic fast mode power spectrum,  $I(\mathbf{k}) \propto k^{-7/2}$  (e.g. Cho & Lazarian 2002). More importantly, the non-linear decorrelation frequency for fast modes,  $v_l k$  (where  $v_l$  is the turbulence velocity on scale  $l$ ), is much smaller than the corresponding linear frequency  $v_A k$ , implying that fast modes decorrelate much more slowly (in turbulence) than Alfvén and slow waves. Furthermore, this non-linearity becomes weaker on smaller scales. Thus, TTD with fast modes will be much less broadened. Figure 3 shows that this results in a velocity diffusion coefficient much more peaked near  $v_{\parallel} \sim v_A$ , closer to the linear theory result. The broadened resonance does still result in a power-law diffusion coefficient at high  $v_{\parallel}$ , with the same power-law indices as in the slow mode case considered above (-2 and -3 for the exponential and Gaussian decorrelation models, respectively). However, the distinction between the exponential and Gaussian models only becomes apparent at very high  $v_{\parallel}$ . This high- $v_{\parallel}$  tail proves to be the most important feature of the broadened resonance for calculating heating rates at high  $v_s$ .

Similar modifications to the calculation in §3.2.1 would need to be made in other regimes. For instance, for slow modes with  $\beta < 1$ , Equation 9 would need to be modified by a multiplicative factor  $\sim \beta/(1 + \beta)$  to account for the decreasing magnetic compression of slow modes in this regime. Additionally, one would instead use a dispersion relation  $\omega = \pm c_s |k_{\parallel}|$ . However, we anticipate that the general functional form of the diffusion coefficient is similar to those shown in Figures 2 and 3 in these different

regimes. We will use this generality of the resonance-broadened diffusion coefficients to interpret our test particle simulation results in §6.

### 3.2.3. Type B diffusion: the $\mu \rightarrow 0$ limit

In the  $\mu \rightarrow 0$  limit, magnetic mirror forces become negligible and all diffusion in parallel velocity is due to Fermi Type B interactions, resulting from the tying of particles to moving, curved field lines. In our non-relativistic case, this change in parallel velocity in one coherent interaction with a curved field line will typically be of the order  $\delta v_{\parallel} \sim v_L \sin \theta \sim v_L (\delta B/B_0)$ , where  $\theta$  is the opening angle of the magnetic field line, as illustrated in Figure 1. These interactions will be stochastic, and we estimate a parallel velocity diffusion coefficient by  $D_{\parallel} \sim \delta v_{\parallel}^2/t_{\text{corr}}$ , where  $t_{\text{corr}}$  is the typical time over which a particle experiences correlated field line motion. For a particle with  $|v_{\parallel}| \ll v_L, v_A$ , the decoherence time of interactions will be determined by the outer-scale fluid motions. The elements of field line curvature which provide FTB diffusion may be thought of as essentially Alfvénic fluctuations, because they are most effective when  $\delta \mathbf{B} \perp \mathbf{B}_0$ . For strong Alfvénic turbulence, the decoherence time of a wave-particle interaction at the outer scale will be provided by a combination of two effects: linear propagation and non-linear distortion (eddy turnover). For weaker turbulence, the linear propagation of fluctuations will control the decorrelation of wave-particle interactions. Furthermore, at any instant in time, the outer-scale fluctuations have correlation lengths  $\sim L$ , because the turbulence is driven on this scale. Thus in either case (strong or weak), a good estimate of the wave-particle correlation time is  $t_{\text{corr}} \sim L/v_A$ , the outer-scale wave crossing time. This allows us to estimate the diffusion coefficient

$$D_{\parallel} \sim \frac{v_L^2}{L/v_A} \left( \frac{\delta B}{B_0} \right)^2 \sim \frac{v_L^4}{L v_A} \quad (17)$$

where the second equality follows from assuming that the typical magnetic field perturbation at the outer scale is of order  $\delta B/B_0 \sim v_L/v_A$ , which will be true for Alfvénic turbulence. We could choose to express this in terms of  $\epsilon$ , the turbulence cascade rate, which in Kolmogorov or GS-like turbulence scales as  $\epsilon \sim v_L^3/L$ . However, the large-scale eddies are those most effective at FTB acceleration. The strong turbulence scalings are least likely to be applicable on these large scales, and so we leave the FTB diffusion coefficients explicitly in terms of  $v_L$ .

On the other hand, particles with  $|v_{\parallel}| \gg v_A$  are essentially interacting with a static snapshot of turbulence, and so  $t_{\text{corr}} \sim L/|v_{\parallel}|$ , the particle crossing time of the outer-scale correlation length. This implies

$$D_{\parallel} \sim \frac{v_L^2 |v_{\parallel}|}{L} \left( \frac{\delta B}{B_0} \right)^2 \sim \frac{v_L^4}{L v_A^2} |v_{\parallel}|. \quad (18)$$

We choose a functional form for  $D_{\parallel}$  that asymptotes to the scalings in Equations 17 and 18 in the low- and high-velocity regimes and varies smoothly between these limits:

$$D_{\parallel,FTB} \equiv C_3 \frac{v_L^4}{L v_A} + C_4 \frac{v_L^4}{L v_A^2} |v_{\parallel}|. \quad (19)$$

$C_3$  and  $C_4$  are dimensionless parameters which we will calibrate against test particle simulations in §6.

### 3.2.4. Phase-decorrelation broadening

The discussion in §3.2.1 focuses on the phenomenological idea of wave-particle phase decorrelation as a result of the decay of the resonant wave. However, the changes in parallel velocity which the test particle experiences in the wave-particle interaction will also lead to phase decorrelation. As a particle's parallel velocity changes, its position  $z$  along the magnetic field changes relative to a ballistic trajectory with  $z_b = z_0 + v_{\parallel,0} t$ . The difference  $\delta z = z - z_b$  is given by  $\delta z = \int \delta v_{\parallel} dt$ , where  $\delta v_{\parallel}$  is the change in particle velocity resulting from the acceleration process. When  $\delta z \sim 1/k_{\parallel}$ , the particle has moved completely out of phase with the wave. For parallel velocities which change diffusively, we may estimate that the rms change in parallel velocity is given by  $\delta v_{\parallel, \text{rms}} \sim \sqrt{D_{\parallel} t}$ . Estimating  $\delta z \sim \delta v_{\parallel, \text{rms}} t$ , the typical extra random phase between wave and particle will be  $\phi \sim k_{\parallel} D_{\parallel}^{1/2} t^{3/2} \sim (t/t_{\text{ph}})^{3/2}$ , where the final approximate equality is simply a definition of  $t_{\text{ph}}$ . One could now use this additional decorrelation in an extension of the broadened resonance of Equation 5. However, this introduces a recursive dependence of  $D_{\parallel}$  on itself, seeming to limit the analytical tractability of this approach. For simplicity, we do not include this effect in our analytical model. However, we do consider this effect in interpreting our test particle results.

Using instead  $\phi^2 \sim k_{\parallel}^2 D_{\parallel} t^3$  in the resonance broadening calculation is formally similar to Equation 61 of Weinstock (1969). Yan & Lazarian (2008) also used a similar approach in modelling resonance broadening. The equivalent of  $t_{\text{ph}}$  which they calculate may be found by using a *ballistic* approximation for the particle deviation, rather than a *diffusive* one, so that  $\delta v_{\parallel, \text{rms}} \sim \mu \nabla B t$  (though this deviation is still treated as effectively random over a distribution of particles, in that it may be parallel or anti-parallel to the mean magnetic field), in which case the effective  $t_{\text{ph}}^{-1} \sim k_{\parallel} v_{\perp} M_A^{1/2}$ . This ballistic assumption may be more appropriate for particle transport at early times. (This scaling assumes that  $\delta|B| \propto M_A$ , which is not true for pure Alfvén waves but is the case in MHD turbulence with a significant component of compressive energy.) This  $t_{\text{ph}}$  is essentially identical to the bounce time for a particle of magnetic moment  $\mu$  in a magnetic wave of amplitude  $M_A B_0$  and wavelength  $\sim 1/k_{\parallel}$ .

## 4. HEATING OF A THERMAL DISTRIBUTION

If the evolution of a distribution of test particles satisfies a diffusion equation (as in eqn. 1), we may multiply both sides of this evolution equation by  $m_s v_{\parallel}^2/2$  and integrate over all velocities to find the volumetric heating rate of the particles,

$$\dot{E}_s = \frac{k_B T_s}{2v_s^2} \int d^3v v_{\parallel}^2 \frac{\partial}{\partial v_{\parallel}} \left( D_{\parallel} \frac{\partial f_s}{\partial v_{\parallel}} \right), \quad (20)$$

where  $T_s$  is the temperature of the particle species under consideration,  $k_B$  is Boltzmann's constant, and the distribution is normalized such that  $\int d^3v f_s(v) = n_s$ , the spatial density of particles. For simplicity, we assume that the distributions are Maxwellian, with a thermal

velocity  $v_s = \sqrt{k_B T_s / m_s}$ . We will treat  $T_s = T$  as a constant when we compare heating of different particle species, appropriate for species in temperature equilibrium.

### 4.1. FTB Heating

The parameterization of FTB diffusion in Equation 19, as well as the assumption of a thermal distribution, allows us to calculate the FTB heating rate from Equation 20:

$$\dot{E}_{s, \text{FTB}} = n_{\text{test}} k_B T \frac{v_L^4}{L v_A} \left( \frac{C_3}{v_s^2} + 2 \sqrt{\frac{2}{\pi}} \frac{C_4}{v_s v_A} \right). \quad (21)$$

$n_{\text{test}}$  refers to the number density of the test particles. The  $v_s^{-2}$  dependence of this expression at small  $v_s$  will cause FTB to dominate the heating of low thermal velocity particles ( $v_s \ll c_s$ , as for e.g. minor ions).

### 4.2. TTD Heating: Linear Theory

The linear theory (LT) diffusion coefficient for slow modes is given by

$$D_{\parallel} \propto v_{\perp}^4 \delta(v_{\parallel} \pm v_p), \quad (22)$$

which gives a heating rate

$$\dot{E}_{s, \text{LT}} \propto T v_s^{-1} \exp\left(-\frac{v_p^2}{2v_s^2}\right). \quad (23)$$

For  $v_s \gg v_p$  and species at roughly the same temperature, this heating rate scales as  $v_s^{-1}$ . In the next section, we find that resonance broadening in general implies a shallower dependence on  $v_s$  for the asymptotic heating rate of high- $v_s$  particles.

### 4.3. TTD Heating: Resonance Broadening

Substituting the exponential and gaussian resonance broadening expressions into the heating rate integral in Equation 20 does not lead to a simple analytic integral, and so in our comparison to our test particle simulations we will numerically evaluate Equation 20. However, as we will see, TTD is the dominant contribution to the heating for high velocity particles. Thus we may gain some insight by considering the heating in the  $v_{\parallel} \gg v_p$  limit.

In particular, the exponential decorrelation function gives  $D_{\parallel} \propto v_{\perp}^4 v_{\parallel}^{-2}$  for  $v_{\parallel} \gg v_p$ . This implies a high- $v_s$  heating rate of

$$\dot{E}_{s, \text{TTD}} \propto T, \quad (24)$$

independent of  $v_s$ . Thus, the exponential model leads to more effective heating for high-velocity particles (e.g. electrons) than linear theory. The Gaussian decorrelation function gives  $D_{\parallel} \propto v_{\perp}^4 |v_{\parallel}|^{-3}$  for  $v_{\parallel} \gg v_p$ , on the other hand, which implies a high- $v_s$  heating rate of

$$\dot{E}_{s, \text{TTD}} \propto \frac{T \ln(v_s)}{v_s}, \quad (25)$$

which has a scaling intermediate between the LT and exponential cases, although closer to the linear theory result given that the only difference is the weakly varying  $\ln(v_s)$  factor.



## 5. NUMERICAL METHODS

Our simulations consist of collisionless test particles evolving in isothermal, subsonic MHD turbulence. Our computational approach is quite similar to that of Lehe et al. (2009), apart from two important changes noted below. We present a summary of our methods here; more detail may be found in the earlier paper.

### 5.1. The MHD Integrator

We use the Athena MHD code of Stone et al. (2008) to evolve the turbulence on a 3D Cartesian grid with periodic boundary conditions. The grid is initialized with a uniform background magnetic field  $B_0$  in the  $x$ -direction, with the velocity set to zero everywhere. The initial magnitude of  $B_0$  is set by our choice of  $\beta = \rho c_s^2 / (B_0^2 / 8\pi)$ , where  $\rho$  is the fluid density and  $c_s$  is the sound speed.

We then inject kinetic energy by providing “kicks” to the velocity field, in a method similar to that of Lemaster & Stone (2009). At each timestep, we generate a velocity perturbation  $\delta\mathbf{v}(\mathbf{k})$  with random amplitudes in Fourier space in the range of  $2 \times \frac{2\pi}{L} < k < 4 \times \frac{2\pi}{L}$ , normalized by a decreasing power law in  $k$ , so that the majority of the driving power enters on the largest scale of  $L/2$ . We also remove modes with  $|k_{\parallel}| < 2 \times \frac{2\pi}{L}$ , to avoid parallel correlation lengths longer than  $\sim L/2$ . We enforce  $\delta\mathbf{v}(\mathbf{k}) \cdot \mathbf{k} = 0$ , so that our velocity field is divergenceless, to minimize the excitation of compressible modes (see the discussion at the end of this subsection for more detail on the decomposition of the turbulence in MHD modes). We then normalize  $\delta\mathbf{v}(\mathbf{k})$  so that the net energy input into the turbulence is given by  $\dot{\epsilon}$ .

We ensure that the kicks are time-correlated by implementing an Ornstein-Uhlenbeck (OU) process (Bartosch 2001), given by

$$\delta\mathbf{v}(\mathbf{k}, t + dt) = f\delta\mathbf{v}(\mathbf{k}, t) + \sqrt{1 - f^2}\delta\mathbf{v}'(\mathbf{k}), \quad (26)$$

which has an autocorrelation time (assuming the continuous limit,  $dt \rightarrow 0$ ) given by

$$\langle \delta\mathbf{v}(\mathbf{k}, t_1) \cdot \delta\mathbf{v}(\mathbf{k}, t_2) \rangle = \langle [\delta v_k(t)]^2 \rangle e^{(t_1 - t_2)/t_{\text{corr}}} \quad (27)$$

where  $f = e^{-dt/t_{\text{corr}}}$ ,  $t_{\text{corr}}$  is the correlation time of the driving,  $dt$  is the timestep of the driving routine, and  $\delta\mathbf{v}'$  is a new random field generated by the process in the previous paragraph. We choose to drive on every MHD timestep. The OU process is simply a mean-reverting random-walk. Note that in order for Equation 27 to properly describe the driving statistics, the initial kick  $\delta\mathbf{v}(\mathbf{k}, t = 0)$  must be drawn from the same random distribution as the subsequent  $\delta\mathbf{v}'(\mathbf{k})$ .

Time-correlated driving is critical for two reasons. First, any process that drives turbulence on large scales will be correlated on some typical timescale depending on the underlying physics of the driving process, rather than pure white noise. Thus a time-correlated driving scheme is more representative of the underlying physics of the turbulence. More pragmatically, evolving our test particles in turbulence with  $\delta(t)$ -correlated driving leads to unphysical acceleration of high gyrofrequency particles, because of the high frequency power present in the turbulent driving. To avoid this, Lehe et al. restricted their analysis to test particles interacting with decaying (non-driven) turbulence. Driving via the OU process allows

us to consider particles evolving in saturated turbulence over arbitrary lengths of time.

On physical grounds, we choose to apply a correlation time of order  $L/v_L$ , the eddy turnover time on the outer scale of the turbulence; see §6.6 for a fuller investigation of the dependence of particle heating on the correlation time. Additionally, we must choose  $t_{\text{corr}} \gg \omega_{\text{max}}^{-1}$ , where  $\omega_{\text{max}}$  is the maximum wave mode frequency resolvable in the MHD simulations. Smaller values of  $t_{\text{corr}}$  imply essentially uncorrelated driving and lead to unphysical heating through a resonance with the MHD timestep.

For a simulation with periodic boundary conditions and a velocity field driven on the size of the domain, a particle with arbitrarily high velocity effectively encounters the same eddy repeatedly, as it crosses the box many times before the eddy decorrelates. This is unphysical, and thus we choose a fiducial volume for our simulations of  $\{16L, 2L, 2L\}$ , so that the box is elongated in the direction parallel to  $\mathbf{B}_0$ , and there are approximately 32 uncorrelated eddies along the length of the box. If we use instead a cubical box of side length  $2L$ , we find  $D_{\parallel}$  is unphysically affected by box-crossing for particles with velocities  $v_{\parallel} \gtrsim 10c_s$ . Extending the box to a size of length  $16L$  in the parallel direction allows us accurately evolve particles with velocities up to  $\sim 50c_s$ . This is particularly important for studying the evolution of electrons, corresponding to our high-velocity particles.

The parallel extension comes at the cost of decreased resolution at the smallest scales. However, FTB acceleration is dominated by the largest eddies, and therefore accurately capturing smaller eddies is irrelevant to zeroth order. Similarly, slow-mode TTD has only a logarithmic dependence on the length of the inertial range. Thus we choose to focus computational resources on the larger-scale eddies.

We choose  $\rho = c_s = L = 1$ , but the results of our simulations can be applied to different physical systems by scaling them with appropriate combinations of  $\rho$ ,  $c_s$ , and  $L$ . Thus our turbulence is controlled by three parameters: the specific energy input rate  $\dot{\epsilon}$ , in units of  $c_s^3/L$ ; the ratio of plasma to magnetic pressure  $\beta$ ; and the correlation time  $t_{\text{corr}}$ , in units of  $L/c_s$ .

We note for reference that we have applied the approximate, Fourier-space method of Cho & Lazarian (2003) to decompose the turbulent kinetic energy in our simulations into Alfvénic, slow, and fast mode components. Across the range of driving rates in our simulations at fixed  $\beta = 1$ , roughly 45% of the kinetic energy is in Alfvénic modes and 45% is in slow modes. At lower  $\beta$ , an increasing fraction of the total energy is in slow modes, up to 60% for  $\beta = 0.1$ , while Alfvénic modes lose a corresponding fraction. Fast modes never comprise more than  $\sim 5\%$  percent of the kinetic energy, and a similarly small fraction belongs to motions with  $k_{\parallel} = 0$  which cannot be identified with any MHD wave mode, corresponding to interchange modes. Changing the correlation time also results in somewhat different 2D power spectra; specifically, longer correlation times appear to frequency-match onto low- $k_{\parallel}$  modes, so that when the turbulence saturates there is power in modes which are not directly driven. We discuss this further in Appendix C.

### 5.2. Particle Integration



Our particle integration methods are described in Lehe et al. (2009). Once the turbulence reaches a fully-saturated state, particles are evolved according to the Lorentz force. We describe particles by their charge-to-mass ratio, expressed in the form of the mean gyrofrequency  $\Omega_0 = qB_0/mc$ . The actual gyrofrequency of a particle will vary according to the local value of  $B$ , but in subsonic turbulence,  $\delta B/B_0 < 1$ , so variations in  $\Omega$  are not large. Our simulations use ideal MHD, with the resistivity  $\eta$  set to zero, so the turbulent dissipation is numerical. Thus the electric field is given by  $\mathbf{E} = -\mathbf{v} \times \mathbf{B}/c$ , where  $\mathbf{v}$  is the fluid velocity.

We integrate the particles with the Boris (1970) implicit particle pusher. This method is symplectic and symmetric in time, and conserves energy and adiabatic invariants to machine precision in simulations with constant fields in space and time. We choose a timestep much smaller than the gyroperiod of the particle. We interpolate the MHD fields on the grid to their value at the particle's location using the Triangular-Shaped Cloud (Hockney & Eastwood 1981) method in space and time, while ensuring that the interpolation does not introduce spurious parallel electric fields ( $E_{\parallel} = 0$ ).

We initialize the particles randomly over the simulation volume, assigning them a  $v_{\perp}$  and  $v_{\parallel}$ , where these are measured perpendicular and parallel to the *local* magnetic field.<sup>8</sup> The perpendicular motion of a particle is the superposition of the fast gyration around  $\mathbf{B}$  and a slowly-varying drift velocity,  $v_{\perp} = |\mathbf{v}_{\text{tot}} - \mathbf{v}_D|$ , where  $\mathbf{v}_{\text{tot}}$  is the total perpendicular velocity of the particle and  $\mathbf{v}_D$  is the drift velocity. We thus require knowledge of the local drift velocity to accurately assign  $v_{\perp}$ . We account for the  $\mathbf{E} \times \mathbf{B}$  drift,  $\nabla B$  drift, curvature drift, and the polarization drift. These latter three drifts are typically smaller by a factor of  $\omega/\Omega$ , where  $\omega^{-1}$  is the timescale of a fluctuation, so one might naively expect them to be small in our simulations. However, the curvature drift, approximately given as  $v_D \sim v_{\parallel}^2/\Omega R_c$  (Hazeltine & Waelbroeck 1998), where  $R_c$  is the local radius of curvature of the magnetic field line, can become important at high  $v_{\parallel}$ .

For many of our simulations, we initialize a distribution of particles with fixed  $v_{\perp}$  and a logarithmically-binned distribution in  $v_{\parallel}$  (or vice-versa), to isolate the effects of one variable. In other cases, we initialize particles according to an isotropic Maxwell-Boltzmann distribution:

$$f(v_{\parallel}, v_{\perp}) = (2\pi v_s^2)^{-3/2} \exp\left(-\frac{v_{\parallel}^2 + v_{\perp}^2}{2v_s^2}\right), \quad (28)$$

where  $v_s$  is the typical thermal velocity of the distribution. We summarize fiducial parameters for our simulations in Table 1, and explicitly note elsewhere when different parameters are used.

## 6. TEST PARTICLE DIFFUSION IN SIMULATIONS

We initialize a distribution of particles in  $v_{\parallel}$ ,  $v_{\perp}$  or  $v$ , the magnitude of the velocity. For particles initially within a given bin in  $v_{\perp}$  and  $v_{\parallel}$ , we calculate diffusion coefficients according to the formal definition

$$D_A \equiv \lim_{\delta t \rightarrow \infty} \frac{\langle (\delta A)^2 \rangle}{2\delta t}, \quad (29)$$

<sup>8</sup> Our TSC interpolation scheme means that the local magnetic field is measured on approximately the grid scale.

TABLE 1  
SUMMARY OF FIDUCIAL SIMULATION PARAMETERS

Parameter	Value
$\rho$	1
$c_s$	1
$L$	1
Resolution	$1024 \times 128^2$
Volume	$16L \times (2L)^2$
$\dot{\epsilon}$ ( $c_s^3/L$ )	$0.1^a$
$\beta$	1
$N_{\text{particles}}$	$2^{11} \times 10^3 \simeq 2 \times 10^5$
$\Omega_0$ ( $c_s/L$ )	$10^5$
$t_{\text{corr}}$ ( $L/c_s$ )	1.5

<sup>a</sup>This produces a sonic Mach number of  $\simeq 0.35$ .

where  $A$  is the diffusing quantity. We are typically interested in calculating  $D_{\parallel}$ , the parallel velocity diffusion coefficient. Our fiducial set of results are for  $\beta = 1$  turbulence with  $\dot{\epsilon} = 0.1 c_s^3/L$  (this holds for Figures 4-9). We measure the diffusion coefficients over a time duration from test particle initialization until after the initial ballistic behavior has become diffusive. For simulations presented here, this is typically between 0.1 and 0.75  $L/c_s$  (with shorter durations for higher turbulent amplitudes).

### 6.1. Non-conservation of $\mu$ ?

We assumed throughout our analytic calculation in §3 that  $\mu$  is conserved. We do observe diffusive changes in  $\mu$  throughout our simulations; i.e.,  $\mu$  is not in fact strictly conserved. However, the changes in  $\mu$  we find do not significantly affect our parallel diffusion results or our interpretation of these results. In Figure 4, we plot  $D_{\mu}/\mu^2$  for our fiducial simulation. All parallel velocities experience some diffusive change in  $\mu$ . However, this change is fractionally small until the highest  $v_{\parallel}$ . Furthermore, for particles with  $v_{\parallel} \gg v_{\perp}$ , velocity diffusion is primarily due to FTB, which is independent of  $\mu$ , so that  $\mu$  changes significantly only in regimes where it is irrelevant to the dynamics. Moreover, the diffusion coefficient for  $\mu$  is fractionally much smaller than the corresponding diffusion coefficient for  $v_{\parallel}$ . Thus we are justified in using the approximation that  $\mu$  is conserved.

### 6.2. Diffusion in $v_{\parallel}$

Figure 5 shows our calculated  $D_{\parallel}$  for particles with  $v_{\perp} = 0.3 c_s$  (solid line). Our fiducial value of  $\dot{\epsilon}$  is sufficiently small that  $\mu \nabla B$  forces are almost negligible for small values of  $v_{\perp}$  and therefore diffusion is dominated by FTB. (A similar run with  $v_{\perp} = 0.1 c_s$ , not shown, is essentially identical.) At low  $v_{\parallel}$ , the diffusion coefficient saturates to a constant value of order  $v_L^4/L v_A \sim 0.005 c_s^3/L$ , consistent with Equation 17 (though a factor of  $\sim 4$  smaller). At high  $v_{\parallel}$ , the diffusion coefficient is proportional to  $v_{\parallel}$ , consistent with our analytic derivation in Equation 18.

Figure 5 also shows that for particles with larger  $v_{\perp}$  (larger  $\mu$ ),  $D_{\parallel}$  is significantly larger for particles with  $v_{\parallel} \lesssim v_{\text{slow}}$ , the phase velocity of slow modes. This is due to TTD, which increases in importance for larger  $\mu$ . In particular, for larger  $v_{\perp}$ , the TTD contribution manifests itself as an approximately constant  $D_{\parallel}$  for  $v_{\parallel} \lesssim$

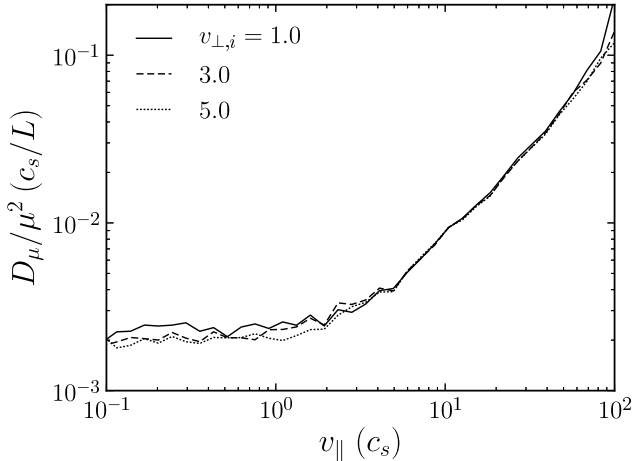


FIG. 4.— Diffusion coefficient for the magnetic moment  $\mu$ , for several values of the initial perpendicular velocity. Diffusion in  $\mu$  is fractionally much smaller than diffusion in  $v_{\parallel}$ ; furthermore, changes in  $v_{\perp}$  are dominated by local variations in the magnetic field rather than the observed slow diffusion in  $\mu$ . Thus in general we are justified in approximating the magnetic moment as a conserved quantity.

$v_{\text{slow}}$ , and then as a smooth decrease in  $D_{\parallel}$  for higher parallel velocities. This is consistent with the resonance broadening TTD models in §3.2.1.

For particles with  $v_{\parallel} \gg v_{\perp}$  beyond the linear resonance at  $v_{\parallel} = v_{\text{slow}}$ , FTB begins to again dominate the parallel velocity diffusion. The high  $v_{\parallel}$  scaling of  $D_{\parallel}$  is  $\propto v_{\parallel}$ , consistent with Equation 18. The importance of FTB can also be seen by the fact that all of the curves in Fig 5 are the same at high  $v_{\parallel}$ , independent of  $v_{\perp}$ . This is because FTB rather than TTD provides the dominant source of velocity diffusion at high  $v_{\parallel}$ , and the value of  $v_{\perp}$  ( $\mu$ ) is irrelevant to the efficiency of FTB diffusion.

The broadened resonance in Figure 5 appears to move to the right for increasing  $v_{\perp}$ . We argue that this is the result of phase-decorrelation broadening, discussed in §3.2.4. We initialize delta-functions in  $v_{\parallel}$ , but as a result of the changes in  $v_{\parallel}$  caused by finite-amplitude turbulence, these bins quickly begin to spread out. We may set the decorrelation time of §3.2.4 equal to  $\omega - k_{\parallel}v_{\parallel} = k_{\parallel}(v_p - v_{\parallel})$  to find the resulting broadening width  $\Delta v_{\parallel} \equiv v_p - v_{\parallel}$ . The phase-decorrelation model in which the initial particle transport is ballistic in  $v_{\parallel}$  (as indeed we observe at early times) predicts that  $\Delta v_{\parallel} \sim M_A^{1/2} v_{\perp}$ , which is consistent with the test particle results in Figure 5.

Figure 6 shows  $D_{\parallel}$  as a function of  $v_{\perp}$  for a distribution of particles with  $v_{\parallel,i} = 0.2 c_s$ . For high  $v_{\perp}$ , the diffusion coefficient scales like  $v_{\perp}^4$ , consistent with the  $\mu^2$  scaling in Equation 10. This scaling may be understood by noting that  $D_{\parallel} \propto a_{\parallel}^2 \propto (\mu \nabla B)^2$ , where  $a_{\parallel}$  is the instantaneous acceleration felt by a charged particle with magnetic moment  $\mu$ . For smaller  $v_{\perp}$ , as  $\mu \rightarrow 0$ , the diffusion reaches the floor provided by the FTB mechanism. However, we note that at later times, we see shallower power laws in  $v_{\perp}$ . We believe that this is also caused by phase-decorrelation effects due to finite changes in particle  $v_{\parallel}$  discussed §3.2.4.

Figure 7 presents a more quantitative comparison be-

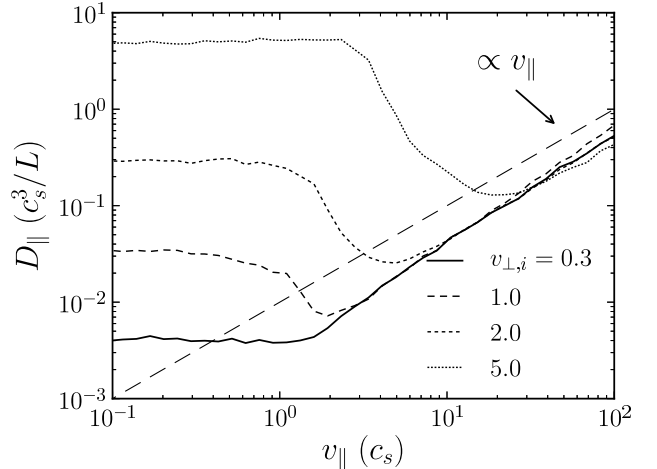


FIG. 5.— Parallel diffusion coefficients as a function of parallel velocity  $v_{\parallel}$  for several values of  $v_{\perp,i}$  (in units of  $c_s$ ) for our fiducial turbulence properties in Table 1. For the lowest  $v_{\perp,i} = 0.3 c_s$  (solid curve), diffusion is provided essentially entirely by the FTB mechanism, which provides an effective floor for  $D_{\parallel}$  at low  $v_{\perp}$ . For higher  $v_{\perp}$ , resonance-broadened transit-time damping causes further diffusion, characterized by a constant  $D_{\parallel}$  below the linear theory resonance at  $v_{\parallel} = v_{\text{slow}} \sim c_s$ , and a smooth falloff above.

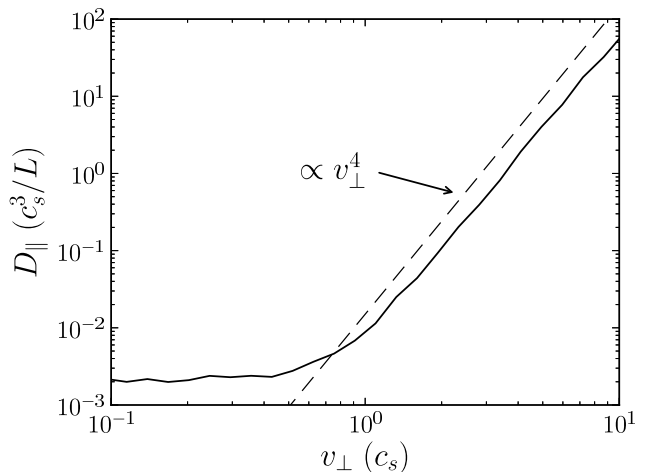


FIG. 6.— Parallel diffusion coefficient measured at early times as a function of perpendicular velocity for a distribution of particles with  $v_{\parallel} = 0.2 c_s$  (other properties of the simulation are summarized in Table 1). At high  $v_{\perp}$ ,  $D_{\parallel} \propto v_{\perp}^4$ ; this is due to transit-time damping. At low  $v_{\perp}$ , the diffusion reaches a floor provided by the Fermi Type-B mechanism. At later times, we see shallower power laws in  $v_{\perp}$ . We believe that this is caused by phase-decorrelation effects; see §3.2.4.

tween our numerical test particle results and the analytic results for  $D_{\parallel}$  derived in §3.2.1. The curve labeled by TTD refers to diffusion with a functional form provided by the Gaussian decorrelation prescription of Equation 13. FTB refers to the sum of the contributions of eqs. 17 and 18. The normalization of the analytic diffusion coefficients are chosen by eye so as to provide the best match to the numerically determined diffusion coefficients. Our analytic model captures the qualitative character of the test particle results.

Figure 8 shows the time dependence of our test particle

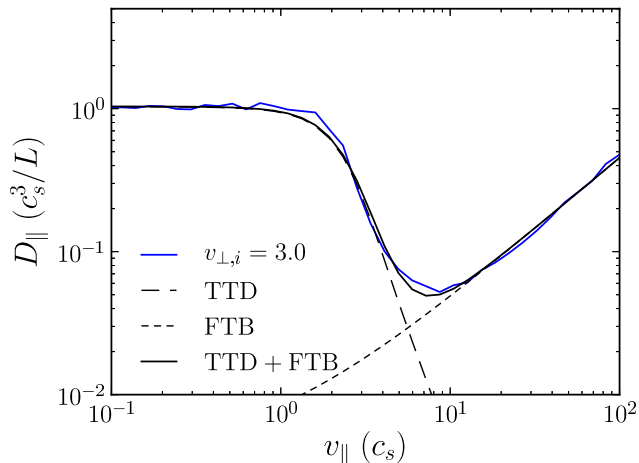


FIG. 7.— Comparison of numerically calculated diffusion coefficients to analytical scalings (using the Gaussian decorrelation model with  $\gamma = 0.5$ ), for a simulation with  $v_{\perp,i} = 3.0c_s$ . The turbulence properties are given in Table 1. TTD dominates at low  $v_{\parallel}$ , while FTB dominates at high  $v_{\parallel}$ .

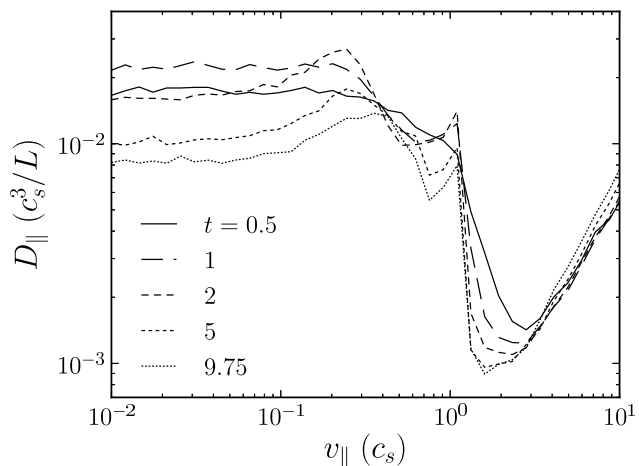


FIG. 8.— Parallel velocity diffusion coefficient vs.  $v_{\parallel}$ , measured at several different times (in units of  $L/c_s$ ), for a simulation with  $\epsilon = 0.01c_s^3/L$ ,  $v_{\perp,i} = c_s$ , and  $t_{\text{corr}} = 3L/c_s$ , approximately equal to the eddy turnover time.

diffusion coefficients measured over different time baselines, for a simulation with  $\epsilon = 0.01c_s^3/L$  and  $v_{\perp} = c_s$ . Perfectly overlying curves measured at different times would indicate perfectly diffusive behavior. We observe time dependence which is generally not perfectly diffusive, and is typically somewhat subdiffusive, in that e.g.  $\langle(\delta v_{\parallel})^2\rangle$  scales somewhat less than linearly with  $t$ .

### 6.3. Approach to quasilinear theory?

For smaller turbulence amplitudes, one might in principle expect the velocity diffusion coefficient to approach the sharp resonance of quasilinear theory, because the turbulence becomes increasingly weak on the outer scale. For example, in the simulation plotted in Figure 8, the amplitude of the turbulence is such that the turbulence is weak on the outer scale, with  $v_L \simeq 0.16c_s \ll v_A$ . Our model of a weak turbulence cascade in Appendix B

predicts a rather sharp resonance, for these parameters. However, no obvious resonance is present in the test particle results shown in Figure 8.

We believe that this is the result of phase-decorrelation broadening, as discussed in §3.2.4. This decorrelation effect acts in addition to the primary wave-decay decorrelation model discussed in this paper. In turbulence, as discussed in §3.2.4, there is a typical wave-particle phase decorrelation time given by  $t_{\text{ph}}^{-1} \sim k_{\parallel}^{2/3} D_{\parallel}^{1/3}$  (if the particle velocity change is diffusive) or  $t_{\text{ph}}^{-1} \sim k_{\parallel} v_{\perp} M_A^{1/2}$  (if ballistic), and we can use this to predict a broadening width  $\Delta v_{\parallel}$  by equating the linear frequency with the decorrelation frequency, as in §6.2.

For the diffusive phase-decorrelation broadening,  $\Delta v_{\parallel} \sim (D_{\parallel}/k_{\parallel})^{1/3}$ . For the results in Figure 8, this approach predicts  $\Delta v_{\parallel} \sim 0.09c_s$ , evaluated at  $k_{\parallel} = 4\pi/L$ . This is well less than the measured broadening. On the other hand, the ballistic (bounce-time) phase-decorrelation broadening gives  $\Delta v_{\parallel} \sim v_{\perp} M_A^{1/2} \sim 0.34c_s$ , which is consistent with the measured broadening to within a factor of  $\sim 2$ . We also note that the double-peaked features in  $D_{\parallel}$  in Figure 8 are similar to those plotted in Appendix A, where we consider the interaction of test particles with one ideal wave.

### 6.4. Heating rate in test-particle simulations

In order to make a quantitative comparison between our analytical heating rates and our test particle calculations, we will use the explicitly parameterized diffusion coefficients of Equations 10, 13, and 19, corresponding respectively to our exponential-decorrelated TTD, Gaussian-decorrelated TTD, and FTB models. Throughout this section, we will generally assume all species are at a constant reference temperature of  $kT = m_s v_s^2$ . Thus the important scaling is with respect to  $v_s$  (or  $m_s$ , equivalently). We choose  $\gamma = 1$  and  $\gamma = 0.5$  for the exponential and Gaussian decorrelation models, respectively, as these values provide a reasonable fit to our simulations.

We simulate distributions of particles that are Maxwellian in  $v = (v_{\perp}^2 + v_{\parallel}^2)^{1/2}$ , and calculate their heating rate  $\dot{E} \equiv (E_f - E_i)/(t_f - t_i)$ . We normalize the initial energy density of the distribution to  $3/4 \rho c_s^2$ , so that the test particles represent the energy of the ions or electrons in a proton-electron isothermal MHD fluid. (Because we use test particles, all of our heating rates may be straightforwardly adapted to a different particle density by multiplying by a factor  $\rho_{\text{test}}/\rho$ .) We calculate a numerical heating rate by fitting a straight line to the test particle energy as a function of time, from  $t = 0.25 - 1L/c_s$ .

We then determine the coefficients  $\{C_1, C_2, C_3, C_4\}$  in the analytic models for  $D_{\parallel}$  by comparison to the test particle diffusion coefficients. For each value of  $\epsilon$ , we focus on the value of  $v_{\perp}$  where our Gaussian analytic model best matches the location of the high- $v_{\parallel}$  cutoff in the parallel diffusion coefficient (in e.g. Figure 7, this cutoff is around  $v_{\parallel} \sim 2c_s$ ). Then we choose the  $C_i$  to match the normalization. The normalization of the analytic curve in Figure 7 is a result of this procedure.

Finally, we calculate the associated “analytic heating

TABLE 2  
SUMMARY OF DIMENSIONLESS CONSTANTS  $C_i$  ( $\beta = 1$ )<sup>a</sup>

<sup>a</sup>These constants normalize the diffusion coefficients given by Equations 10, 13, and 19.

	$\dot{\epsilon} = 0.01$	$\dot{\epsilon} = 0.1$	$\dot{\epsilon} = 1$
$C_1$	0.085	0.07	0.065
$C_2$	0.15	0.12	0.11
$C_3$	0.25	0.17	0.2
$C_4$	0.5	0.3	0.4

rates” by numerically evaluating the integral in Equation 20 (integrating the diffusion equation over parallel and perpendicular velocities) using our fits for the dimensionless coefficients  $C_i$ . We expect the  $C_i$  to depend only weakly on parameters of the turbulence such as  $\dot{\epsilon}$ ,  $L$ , etc. In Table 2, we provide our approximate values for these normalization coefficients for three runs at  $\dot{\epsilon} = 0.01, 0.1$ , and  $1 c_s^3/L$ , all at  $\beta = 1$ ; we discuss the dependence on  $\beta$  in §6.5. Over a factor of 100 in  $\dot{\epsilon}$ , the  $C_i$  do not change significantly.

Figure 9 shows how the analytic heating rates compare to our test particle results for several different values of  $\dot{\epsilon}$ . Our numerically calculated heating rates never asymptote to a constant at high- $v_s$ . It is thus clear that the Gaussian decorrelation function (orange curves) provides a better fit to the simulation data (black curves) in the high- $v_s$  regime, where it scales as  $\ln(v_s)/v_s$ , as opposed to the exponential decorrelation prescription (blue curves), which is independent of  $v_s$ . Similarly, the delta function heating rate (pink curves) are typically too steep. In the high velocity regime, the heating rates are reasonably well-fit by a functional form  $\dot{\epsilon}_{\text{part}} \simeq 0.33 v_L^2 (v_s/c_s)^{-0.4}$ , though this expression only applies for  $\beta = 1$ .

The dominant heating mechanism in Figure 9 depends on the thermal velocity of the test particles. Above the linear theory resonance at  $v_{\parallel} \sim v_{\text{slow}}$ , the TTD contribution to the diffusion coefficient scales like  $\mu^2/v_{\parallel}^{\alpha} \propto v_{\perp}^4/v_{\parallel}^{\alpha}$ , where  $\alpha = 2$  or  $3$  depending on the decorrelation model. Thus, in the bulk of an isotropic thermal distribution, where  $v_{\perp} \sim v_{\parallel} \sim v_s$ , TTD is increasingly important at higher  $v_s$ . For low thermal velocity particles, on the other hand,  $\mu \rightarrow 0$  and FTB dominates.

As discussed in §4, linear theory implies an asymptotic heating rate  $\dot{E} \propto v_s^{-1}$  for high  $v_s$ . This in turn implies that electrons, with thermal velocity  $v_e = \sqrt{m_p/m_e} v_p \simeq 43 v_p$  (where  $m_p$  and  $v_p$  are respectively the mass and thermal velocity of protons) are heated much less effectively than protons by the compressive fluctuations in  $\beta \sim 1$  MHD turbulence. In Table 3, we provide estimates of  $\dot{E}_p/(\dot{E}_p + \dot{E}_e)$ , the proton-to-total heating ratios in our test particle simulations, for a range of  $\dot{\epsilon}$  and  $\beta$ . We assign protons a value of  $v_s = c_s/\sqrt{2}$ , appropriate for an equal-temperature electron-proton plasma. These calculations indicate that the electron heating rate is typically smaller than the proton heating rate by a factor of 2-5, rather than 43. This is primarily due to the asymptotic  $\ln(v_s)/v_s$  scaling of the simulated heating rates, corresponding to our Gaussian decorrelation model (see eqn. 25). It is interesting to note that the proton-to-total

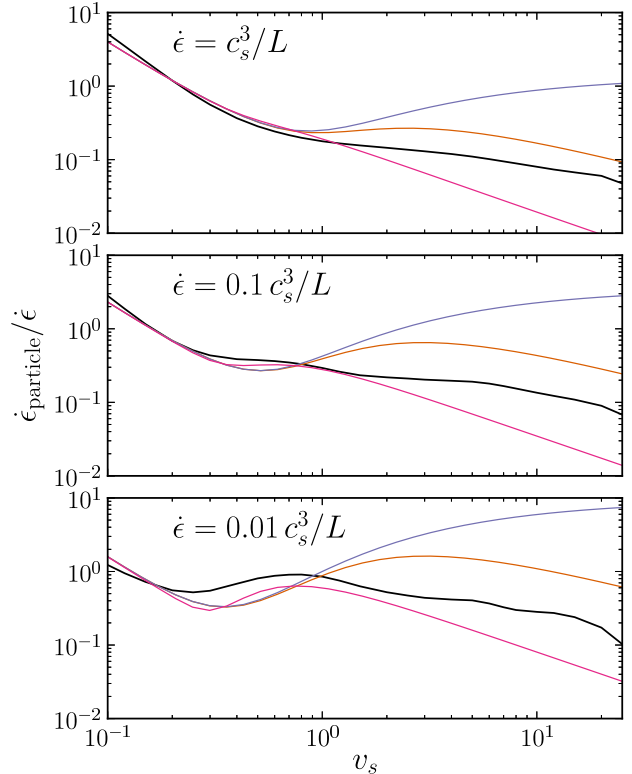


FIG. 9.— Test particle heating rate as a function of test particle thermal velocity  $v_s$ , for  $\beta = 1$  and several different values of the turbulence driving rate  $\dot{\epsilon}$ ; we also show a comparison to our analytically predicted heating rates from §4. Black curves correspond to test particle results, blue curves correspond to an exponential decorrelation model (see eqn. 24), orange curves correspond to Gaussian decorrelation (eqn. 25), and pink curves to a purely linear theory diffusion coefficient. In each case, FTB heating dominates at low  $v_s$ , while TTD dominates at high  $v_s$ . The Gaussian decorrelation model provides a notably more accurate scaling at high  $v_s$  than the exponential model. At lower  $\dot{\epsilon}$ , the delta-function heating rate becomes more plausible; this is consistent with the idea that the turbulence is weaker in these simulations. Test particle heating of e.g. protons with  $v_s = c_s/\sqrt{2}$  is within a factor of 4 of the turbulent cascade rate  $\dot{\epsilon}$  in all cases. See §6.4 for a more detailed discussion.

TABLE 3  
PROTON-TO-TOTAL HEATING RATIO IN TEST PARTICLE SIMULATIONS

$\dot{E}_p/(\dot{E}_p + \dot{E}_e)$	$\dot{\epsilon}(c_s^3/L)$	$\beta$
0.84	1	1
0.84	0.1	1
0.85	0.01	1
0.81	0.1	3
0.74	0.1	0.3
0.69	0.1	0.1

heating rates we find are consistent with empirical inferences of proton vs. electron heating in the solar wind (Cranmer et al. 2009), both in magnitude and in the increasing electron heating for smaller  $\beta$ .

In Figure 9, our analytic calculations with Gaussian resonance broadening overestimate the magnitude of the TTD heating at high  $v_s$ , particularly for smaller  $\dot{\epsilon}$ . This is for two reasons. The first is that we fit heating rates

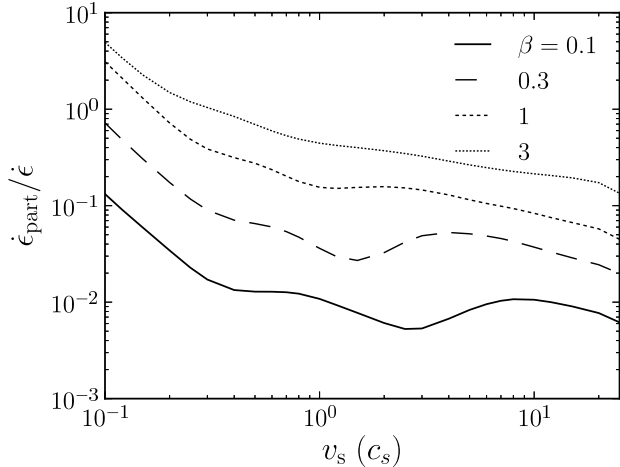


FIG. 10.— Test particle heating rate as a function of test particle thermal velocity  $v_s$  for several different values of plasma  $\beta$  at fixed kinetic energy input rate  $\dot{\epsilon} = 0.1 c_s^3/L$ .

over the baseline  $t = [0.25, 1] L/c_s$ . However, because the distributions are driven away from isotropy, the heating rate becomes less efficient over time, and so the test particle energy increases somewhat sub-linearly. Our analytics assume instead an isotropic Maxwellian at the original thermal velocity.

A more important effect is that the analytic model used in Figure 9 is purely strong turbulence, with  $\omega_{\text{nl}} \sim \omega_{\text{linear}}$  (see §3.2.1). However, the turbulence in the simulations with lower  $\dot{\epsilon}$  is in fact weaker, with  $\omega_{\text{nl}} < \omega_{\text{linear}}$ . We consider the diffusion coefficients resulting from a combination of weak and strong turbulence in Appendix B; this results in a sharper resonance which approaches the delta-function of linear theory in the  $M_A \rightarrow 0$  limit. Thus we might expect a heating rate closer to the linear theory heating rate (the pink curves in Figure 9) for the runs with smaller  $\dot{\epsilon}$ , as indeed is the case in Figure 9. However, this interpretation is complicated by the fact that we do not find a clear peak in the test particle velocity diffusion coefficients at low  $\dot{\epsilon}$  (see Figure 8). This is likely due to phase-decorrelation broadening, as discussed in §3.2.4.

### 6.5. Dependence on $\beta$

Figure 10 shows the simulated heating rates for a thermal distribution of particles for several different values of plasma  $\beta$  at fixed  $\dot{\epsilon} = 0.1 c_s^3/L$ , measured over a longer baseline of  $t = [1, 5] L/c_s$ . We do not attempt to make a quantitative comparison with our analytic model. However, qualitatively, three effects are clear. First, FTB heating at low  $v_s$  decreases in effectiveness at low  $\beta$ . This is due to the decreasing curvature of the typical magnetic field line involved in FTB interactions:  $v_L/v_A$  decreases as  $\beta$  decreases at fixed sound speed and  $\dot{\epsilon}$ .

Second, the contribution of slow modes to TTD decreases with decreasing beta. The fraction of the slow mode energy in parallel magnetic field compressions is  $\propto \beta/(\beta + 1)$ . Thus, at low  $\beta$  TTD heating due to the slow modes becomes less important.

Finally, for  $\beta = 0.1$ , there is a clear bump in the heating rate at high thermal velocities, which moves to lower  $v_s$  at higher  $\beta$ . We associate this peak with TTD heating

by fast modes, which have a phase velocity approaching  $v_A$  in the low- $\beta$  limit. The reduced heating in the  $\beta = 0.1$  case relative to the  $\beta = 0.3$  is simply due to the fact that our simulations have a greatly reduced proportion of fast mode energy at lower  $\beta$ , by a factor of  $\sim 3$ .

### 6.6. Dependence on driving correlation time

Figure 11 shows the heating rate of a thermal distribution for different  $t_{\text{corr}}$ , the correlation time of the Ornstein-Uhlenbeck process with which we drive the turbulence. Over a factor of  $\sim 400$  in  $t_{\text{corr}}$ , there is only a factor of  $\sim 4$  change in the heating rate; this suggests that to zeroth order, our results are insensitive to the value of  $t_{\text{corr}}$ . However, when  $t_{\text{corr}} \rightarrow t_{\text{MHD}}$  (not shown in Fig. 11), where  $t_{\text{MHD}}$  is the MHD timestep, we find that our results approach the limit of an uncorrelated driving scheme (typically,  $t_{\text{MHD}} \sim 8 \times 10^{-4} L/c_s$  in our highest resolution simulations). In this limit, we find acceleration mimicking the cyclotron resonance for high-gyrofrequency particles which should not be resonant, because of the artificially high frequencies introduced by the driving (see also Lehe et al. 2009).

Increasing  $t_{\text{corr}}$  from this minimum value while fixing other properties of the turbulence systematically affects the turbulent kinetic energy in each of the MHD modes. The other physically relevant timescale in our calculations is the outer-scale eddy turnover time, which for our fiducial simulation (see Table 1) is approximately  $t_{\text{eddy}} \sim L/v_L$ , which is approximately given by  $\sim 3 L/c_s$  for the fiducial case. Again applying the Fourier spectral decomposition of Cho & Lazarian (2003), increasing  $t_{\text{corr}}$  from  $0.01 L/c_s$  to  $4.0 L/c_s$  decreases the Alfvénic energy from 55% to 45%, decreases the fast mode energy from 15% to 3%, and increases the slow mode energy from 30% to 45% (while decreasing the overall kinetic energy in the turbulence by roughly 30%). Note that we hold the input power  $\dot{\epsilon}$  fixed as  $t_{\text{corr}}$  varies.

We also find that despite driving no modes with parallel wavelengths longer than  $L/2$ , long-wavelength modes with  $k_{\parallel} v_A \sim t_{\text{corr}}^{-1}$  naturally appear in the developed turbulence. We believe that this is due to frequency-matching between the correlation time of the driving and the natural frequency of long-parallel-wavelength modes (see Appendix C).

These varying proportions of energy affect the thermal heating rate in ways which are largely consistent with our interpretation of the heating (see Fig. 11). The decreasing energy in fast modes manifests itself in a factor of  $\sim 4$  decrease in the TTD heating rate at high thermal velocity, while the increase in slow mode energy contributes to increasing the heating rate just below  $v_s \sim c_s$ . The decrease in FTB heating is consistent with the decrease of  $v_L$  at longer correlation times.

### 6.7. Non-thermal acceleration?

In previous sections, we have focused on short-timescale interactions between particles and turbulence to calculate diffusion coefficients and corresponding heating rates. On longer timescales, it is unclear whether these interactions produce a thermal or non-thermal evolution of the distribution function. To investigate this question, we carried out test particle simulations lasting for longer times.

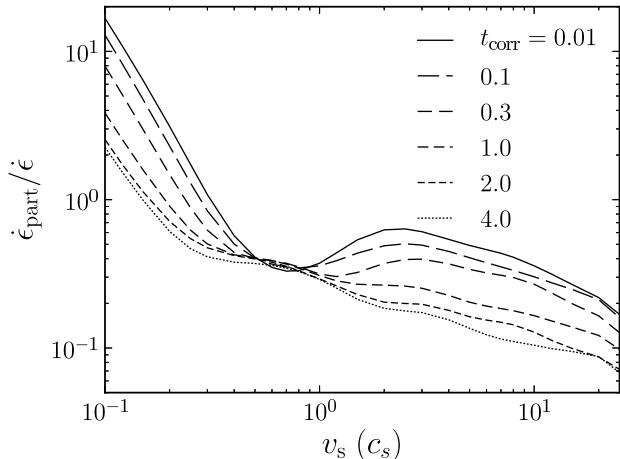


FIG. 11.— Test particle heating rate as a function of test particle thermal velocity  $v_s$  for several different values of the OU turbulent driving correlation time,  $t_{\text{corr}}$ , in units of  $L/c_s$ . All other parameters are our fiducial parameters, listed in Table 1. Changes in the heating rate are largely due to varying proportions of energy in the MHD modes (see §6.7), but the overall results are consistent at the factor of  $\sim 4$  level over a factor of  $\sim 400$  change in  $t_{\text{corr}}$ . The large-scale eddy turnover time corresponds to  $t_{\text{corr}} \sim$  a few  $L/c_s$ .

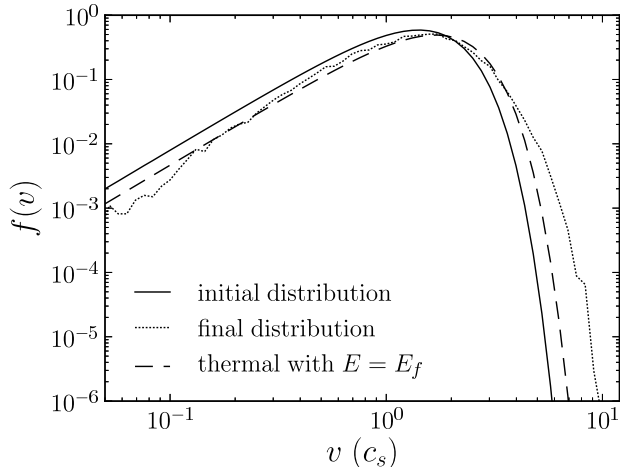


FIG. 12.— The distribution function of an initially thermal distribution of test particles with  $v_s = c_s$  evolving in turbulence with  $\beta = 1$  and  $\dot{\epsilon} = 0.1$ , plotted at  $t = 0$  (solid curve) and  $t = 20 L/c_s$  (dotted curve); this corresponds to  $\sim 10$  eddy turnover times of the turbulence. We also plot a thermal distribution with the same energy as the final distribution (long dashed curve). The distribution becomes mildly non-thermal due to the turbulent diffusion, but TTD does not lead to a power-law tail.

Figure 12 shows the distribution function (dotted curve) resulting from a simulation with  $\dot{\epsilon} = 0.1 c_s^3/L$  run for  $t = 20 L/c_s$ , corresponding to several eddy turnover times. The thermal energy of the particles has increased by  $\sim 50\%$ . For comparison, Figure 12 also shows a Maxwellian with the same energy as the final distribution (long dashed curve). The final distribution is clearly non-thermal, in that there is somewhat more energy in high-velocity particles, and less for low-velocity particles. However, the distribution is only weakly non-thermal, in that there is no evidence for the formation of a power-law tail at high velocities.

This weak non-thermality is not that surprising, as even our broadened TTD resonance diffusion coefficient is largest for particles with  $v_{\parallel} \sim v_A$ . Our result is inconsistent with recent work claiming that compressible turbulence generically leads to non-thermal power law tails  $f(v) \propto v^{-5}$ , as observed in the solar wind (see Fisk & Gloeckler 2007, 2008). However, their formalism assumes an isotropic or nearly isotropic distribution function, enforced by particle collisions or microscale instabilities, and has been criticized by Jokipii & Lee (2010) and Schwadron et al. (2010), among others. We will investigate this point in more detail in future work.

## 7. CONCLUSIONS

We have studied the interaction between charged test particles and low-frequency, large-scale MHD turbulence. This interaction is important in a wide range of astrophysical systems, including the solar wind and cosmic ray transport through the galaxy. The coupling between particles and MHD turbulence leads to velocity-space evolution of the particles, including diffusion, heating, and acceleration. We have used simple physical arguments to motivate analytic models of resonance broadening due to the interaction between particles and strong turbulence (§3.2.1). Furthermore, we have shown that the non-resonant interaction of charged particles with moving, curved magnetic field lines (see Fig. 1) is important for a full understanding of the velocity-space diffusion of particles in a turbulent plasma (§3.2.3).

We have calibrated these analytic models of velocity space diffusion against simulations of charged test particles in fully dynamical MHD turbulence (§6). These calibrations are summarized in Equations 10 and 13, and Table 2. We anticipate that these calibrations of the velocity space diffusion of test particles in MHD turbulence will be useful for a wide range of future astrophysical and heliospheric applications.

Our most important results include:

- *The transit-time damping resonance is highly broadened in MHD turbulence*, relative to the delta-function prediction of linear theory. Our phenomenological model for resonance broadening, which describes wave decoherence in strong MHD turbulence, generically leads to a velocity diffusion coefficient which approaches a constant at low- $v_{\parallel}$  and a high- $v_{\parallel}$  power-law tail (see Fig. 2). We also see evidence for phase-decorrelation broadening, in which finite-amplitude turbulence accelerates particles into and out of resonance over relatively short timescales (see §3.2.4). The significant broadening we find implies that many particles, not just particles moving with the phase velocity of the waves, can strongly interact with the turbulence. Presumably this conclusion would also apply to the Landau resonance in turbulence with parallel electric fields, although in this study we have limited our considerations and simulations to ideal MHD.
- *Heating rates for high thermal velocity particles are inconsistent with a slow mode decorrelation model which is exponential in time* (i.e., a Lorentzian resonance function). A Gaussian model for slow mode decorrelation produces heating rates at high thermal velocities which are much more consistent with

our test particle calculations (see Fig. 9). Because of their weaker nonlinearity and longer decorrelation time, we are not able to distinguish between the exponential and Gaussian decorrelation models for fast modes.

- *Fermi Type-B interactions*, wherein particles are slung around by moving, curved magnetic field lines (see Fig. 1), are critical in describing the full velocity space diffusion of charged particles with MHD turbulence (see §3.2.3 and Fig. 5). These interactions have a non-resonant character, and accelerate particles independent of the particles' magnetic moment  $\mu$ . In general, FTB dominates for particles with low  $\mu$  (where the TTD interactions become correspondingly weak) or for particles with  $v_{\parallel} \gg (v_A/v_L)^{1/2} v_{\perp}$  (such that even the broadened TTD resonance has fallen off significantly).
- FTB dominates the heating of particles with thermal velocities  $v_s$  much less than the fast and slow mode phase speeds, while TTD dominates the heating of high- $v_s$  particles (see Fig. 9). FTB heating is thus particularly important for minor ions which have thermal velocities less than the plasmasound speed. For our fiducial case, with  $M_A$  similar to the solar wind, FTB and TTD contribute a similar amount of heating to protons.
- *TTD can efficiently damp the turbulent energy in compressive MHD modes*: we find test particle heating rates comparable to the turbulent energy cascade rate for a wide range of plasma parameters (see Fig. 9). Furthermore, electron heating is comparable to proton heating for the range of  $\beta \sim 0.1 - 3$  we studied (see Table 3). Our estimated proton-to-total heating ratios are consistent with empirical studies in the solar wind (Cranmer et al. 2009). We note, however, that our calculations do not include processes that damp the Alfvénic component of the turbulent fluctuations at small scales and so do not capture all of the heating that is likely important in the solar wind and other astrophysical plasmas.
- *MHD turbulence does not efficiently accelerate collisionless test particles* out of the bulk of a thermal distribution (see Fig. 12). We find no evidence for the formation of a power-law tail even after many turnover times of the turbulence on large scales. Instead, most of the turbulent energy is converted into thermal energy of the bulk of the plasma.

In our simulations,  $\sim 45 - 50\%$  of kinetic energy is in slow modes, while  $\sim 3 - 5\%$  is in fast modes. As mentioned in §5, this is notably higher than in the near-Earth solar wind, where  $\sim 10\%$  of energy is in slow modes and a negligible fraction is in fast modes (Howes et al. 2011a). Because compressive wave modes heat test particles so efficiently (at a rate generally comparable to the turbulent cascade rate  $\dot{\epsilon}$ ), any energy initially in those modes would be quickly damped out. This is consistent with the fact that the solar wind contains a smaller proportion of

compressive energy in the inertial range than naive ideal MHD simulations.

We also find that the Alfvénic component of the turbulent cascade will be significantly damped by Fermi Type-B interactions at the outer scale where the turbulence spectrum is nearly isotropic. However, FTB interactions quickly become weak on smaller scales, and so their effect on the inertial range of the turbulence can probably be neglected. Transit-time damping, on the other hand, damps energy out of all decades in wavenumber at equal rates, but requires energy in compressive modes to be effective.

Another interesting consequence of FTB interactions is that velocity diffusion depends only on the turbulence properties, and is independent of particle mass or charge. This implies that the heating time,  $t_h \sim nk_B T / \dot{E}$ , is independent of particle mass and charge. The cooling or expansion time  $t_c \sim r/v_{sw}$  in the solar wind is also independent of particle mass and charge (where  $r$  is the heliocentric distance and  $v_{sw}$  is the expansion velocity of the solar wind). If  $t_h \gg t_c$ , the particles will simply cool by adiabatic expansion, and their final temperatures will be determined by their initial temperatures. However, if  $t_h \ll t_c$ , then the particles will quickly heat up until  $t_h \sim t_c$ . If we assume that FTB interactions are the most important heating process for minor ions, this balance implies a temperature which is independent of charge but proportional to the species mass,  $T_s \sim m_s v_L^4 r / (k_B L v_A v_{sw})$ .

The interaction between particles and compressive MHD turbulence has been invoked to explain the  $v^{-5}$  distribution at high velocities observed in the solar wind (Fisk & Gloeckler 2007, 2008). Our results are not consistent with these models in that we see no evidence for the development of a power-law tail to the distribution function even after many turnover times on large scales (see Fig. 12 and §6.7).

In future work, we intend to implement simple pitch-angle scattering of test particles, mimicking the effects of small-scale plasma instabilities such as the firehose and mirror instabilities. It will be interesting to assess whether our results on particle acceleration and the long-term evolution of the distribution function change in the presence of significant pitch-angle scattering. In addition, our test particle methods are sufficiently general that they may be applied in simulations of turbulence which are relevant on smaller scales, e.g. Hall MHD turbulence, to probe the gyroscale transition in the solar wind.

We thank a very helpful anonymous referee, whose suggestions greatly improved the paper. This material is based on work supported by the National Science Foundation Graduate Research Fellowship under Grant No. DGE-1106400. Additionally, this work was supported in part by NSF-DOE grant PHY-0812811, NASA HTP grant NNX11AJ37G, and NSF grant ATM-0752503. Computing time was provided by the National Science Foundation TeraGrid/XSEDE resource on the Kraken and Frost supercomputers. Additional computations for this paper were performed on the Henyey cluster at UC Berkeley, supported by NSF grant AST-090580.



## REFERENCES

- Bartosch, L. 2001, *International Journal Of Modern Physics*, 12, 851
- Beresnyak, A. 2011, *Physical Review Letters*, 106, 18
- . 2012, *Monthly Notices of the Royal Astronomical Society*, 422, 3495
- Bieber, J. W., Matthaeus, W. H., Smith, C. W., Wanner, W., Kallenrode, M.-B., & Wibberenz, G. 1994, *The Astrophysical Journal*, 420, 294
- Boldyrev, S. 2006, *Physical Review Letters*, 96, 1
- Boris, J. 1970, in *Proceedings of the Fourth Conference on Numerical Simulations of Plasmas*, Naval Research Lab, 3–67
- Chandran, B. D. G. 2000, *Physical Review Letters*, 85, 4656
- . 2003, *The Astrophysical Journal*, 599, 1426
- Chandran, B. D. G., Li, B., Rogers, B., Quataert, E., & Germaschewski, K. 2010, *The Astrophysical Journal*, 720, 503
- Chaston, C. C. 2004, *Journal of Geophysical Research*, 109, 1
- Chen, C. H. K., Mallet, A., Yousef, T. A., Schekochihin, A. A., & Horbury, T. S. 2011, *Monthly Notices of the Royal Astronomical Society*, 415, 3219
- Cho, J., & Lazarian, A. 2002, *Physical Review Letters*, 88, 1
- . 2003, *Monthly Notices of the Royal Astronomical Society*, 345, 325
- Cranmer, S. R., Matthaeus, W. H., Breech, B. A., & Kasper, J. C. 2009, *The Astrophysical Journal*, 702, 1604
- Cranmer, S. R., & van Ballegooijen, A. A. 2003, *The Astrophysical Journal*, 594, 573
- . 2012, *The Astrophysical Journal*, 754, 92
- Cranmer, S. R., van Ballegooijen, A. A., & Edgar, R. 2007, *The Astrophysical Journal Supplement Series*, 171, 520
- Dmitruk, P., Matthaeus, W. H., & Seenu, N. 2004, *The Astrophysical Journal*, 617, 667
- Drake, J. F., Cassak, P. A., Shay, M. A., Swisdak, M., & Quataert, E. 2009, *The Astrophysical Journal*, 700, L16
- Drake, J. F., Swisdak, M., Che, H., & Shay, M. A. 2006, *Nature*, 443, 553
- Dupree, T. 1966, *Physics of Fluids*, 9, 1773
- Fermi, E. 1949, *Physical Review*, 75, 1169
- Fisk, L., & Gloeckler, G. 2007, *Proceedings of the National Academy of Sciences of the United States of America*, 104, 5749
- . 2008, *The Astrophysical Journal*, 686, 1466
- Galtier, S., Nazarenko, S. V., Newell, A. C., & Pouquet, A. 2000, *Journal of Plasma Physics*, 63, 447
- Gary, S. P., & Borovsky, J. E. 2008, *Journal of Geophysical Research*, 113, 1
- Goldreich, P., & Sridhar, S. 1995, *The Astrophysical Journal*, 438, 763
- . 1997, *The Astrophysical Journal*, 485, 680
- Grappin, R., & Müller, W.-C. 2010, *Physical Review E*, 82, 2
- Hazeltine, R., & Waelbroeck, F. 1998, *The Framework of Plasma Physics* (Perseus Books)
- Higdon, J. C. 1984, *The Astrophysical Journal*, 285, 109
- Hockney, R., & Eastwood, J. 1981, *Computer Simulation Using Particles* (CRC Press)
- Howes, G. G., Bale, S. D., Klein, K. G., Chen, C. H. K., Salem, C. S., & TenBarge, J. M. 2011a, 4
- Howes, G. G., Cowley, S. C., Dorland, W., Hammett, G. W., Quataert, E., & Schekochihin, A. A. 2008, *Journal of Geophysical Research*, 113, 1
- Howes, G. G., TenBarge, J. M., & Dorland, W. 2011b, *Physics of Plasmas*, 18, 102305
- Jiang, Y. W., Liu, S., & Petrosian, V. 2009, *The Astrophysical Journal*, 698, 163
- Jokipii, J. R. 1966, *The Astrophysical Journal*, 146, 480
- Jokipii, J. R., & Lee, M. A. 2010, *The Astrophysical Journal*, 713, 475
- Kennel, C., & Engelmann, F. 1966, *Physics of Fluids*, 9, 2377
- Kraichnan, R. H. 1965, *Physics of Fluids*, 8, 1385
- Leamon, R. J., Smith, C. W., Ness, N. F., & Wong, H. K. 1999, *Journal of Geophysical Research*, 104, 22331
- Lehe, R., Parrish, I. J., & Quataert, E. 2009, *The Astrophysical Journal*, 707, 404
- Lemaster, M., & Stone, J. 2009, *The Astrophysical Journal*, 691, 1092
- Lithwick, Y., & Goldreich, P. 2001, *The Astrophysical Journal*, 562, 279
- Maron, J. L., & Goldreich, P. 2001, *The Astrophysical Journal*, 554, 1175
- McChesney, J., Stern, R., & Bellan, P. 1987, *Physical Review Letters*, 59, 1436
- Montgomery, D., & Turner, L. 1981, *Physics of Fluids*, 24, 825
- Ng, C. S., & Bhattacharjee, A. 1997, *Physics of Plasmas*, 4, 605
- Perez, J. C., & Boldyrev, S. 2008, *The Astrophysical Journal*, 672, L61
- Qin, G., Matthaeus, W. H., & Bieber, J. W. 2006, *The Astrophysical Journal*, 640, L103
- Quataert, E. 1998, *The Astrophysical Journal*, 20, 978
- Quataert, E., & Gruzinov, A. 1999, *The Astrophysical Journal*, 520, 248
- Schwadron, N. A., Dayeh, M. A., Desai, M., Fahr, H., Jokipii, J. R., & Lee, M. A. 2010, *The Astrophysical Journal*, 713, 1386
- Shalchi, A., Bieber, J. W., Matthaeus, W. H., & Qin, G. 2004, *The Astrophysical Journal*, 616, 617
- Shalchi, A., & Schlickeiser, R. 2004, *Astronomy & Astrophysics*, 420, 799
- Shebalin, J. V., Matthaeus, W. H., & Montgomery, D. 1983, *Journal of Plasma Physics*, 29, 525
- Stix, T. 1992, *Waves in Plasmas* (Springer)
- Stone, J., Gardiner, T. A., Teuben, P., Hawley, J. F., & Simon, J. B. 2008, *The Astrophysical Journal Supplement Series*, 178, 137
- Verdini, A., & Grappin, R. 2012, *Transition from weak to strong cascade in MHD turbulence*
- Weinstock, J. 1969, *Physics of Fluids*, 12, 1045
- Yan, H., & Lazarian, A. 2004, *The Astrophysical Journal*, 614, 757
- . 2008, *The Astrophysical Journal*, 673, 942

## APPENDIX

## A. LANDAU-TYPE RESONANCE BETWEEN TEST PARTICLES AND ONE WAVE

To consider the effects of particle trapping and bin-crossing on our method for measuring velocity diffusion coefficients, we have simulated a simpler self-contained one-dimensional toy problem, where particles feel a sinusoidal, travelling acceleration of the form  $a = a_0 \sin(kx - kv_p t)$ . This is effectively the Landau problem with test particles. (The toy problem is independent of Athena, but we have confirmed that the results are qualitatively identical to test particles interacting with a single slow mode wave in Athena.)

The mean-square change in the velocity of test particles  $\langle(\delta v)^2\rangle$  for several waves with different amplitudes is shown in Figure 13. We plot  $\langle(\delta v)^2\rangle$  because this quantity converges to a constant at long times. If each bin in  $v$  were truly a delta-function, and there was no numerical loss of accuracy, then  $\langle(\delta v)^2\rangle$  for test particles in a given bin would reach a maximum after approximately  $0.5L/(v - v_p)$  (corresponding to half of the wave-particle interaction time), and then decrease back to zero as every particle returned to its original phase with respect to the wave, though offset by  $2\pi$ . However, because particles are smoothly distributed in velocity within each bin, slight initial velocity differences lead to the destruction of this phase coherence over time, and  $\langle(\delta v)^2\rangle$  converges to a constant value of roughly half its maximum.

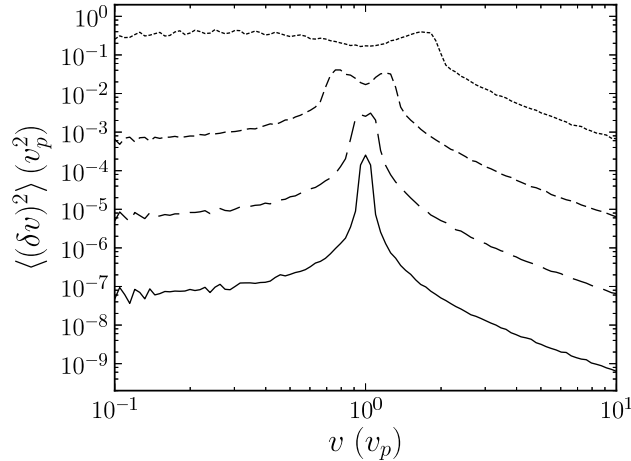


FIG. 13.— Mean-square velocity change for 1D toy problem of test particles interacting with a wave of phase speed  $v_p$ , measured after 60 wave periods (long enough that the plotted quantity has converged). The ratio of the linear wave time to the nonlinear acceleration time (evaluated for particles at the resonance) ranges logarithmically from 0.001 (solid curve) to 1 (dashed curve). For small-amplitude waves, a sharp resonance at  $v_p$  is evident. As the amplitude grows larger, particle trapping effects associated with finite amplitude lead to a broadening of the resonance. A similar effect occurs in MHD turbulence, where finite-amplitude  $\mu\nabla B$  forces move resonant particles off-resonance. We call this effect phase-decorrelation broadening (see §3.2.4).

Acceleration by a small-amplitude wave produces a very sharp resonance around the wave phase velocity, while particle trapping significantly broadens the resonance for large-amplitude waves. For this problem, a small amplitude wave is one for which  $t_{\text{lin}}/t_{\text{acc}} \ll 1$ , where  $t_{\text{lin}} \sim 1/v_p k$  is the linear wave period and  $t_{\text{acc}} \sim v/a_0$  is the time for a particle's velocity to change significantly due to the wave-particle interaction. The transport in velocity space is not truly diffusive for this toy problem, except for particles very near the resonance.

The results of this simple problem are directly analogous to test particles interacting with MHD turbulence. When  $t_{\text{lin}}/t_{\text{ph}} \gtrsim 1$  (where  $t_{\text{ph}}$  is the time required for particles to significantly move out of phase with a wave), particles experience significant acceleration and quickly fall out of phase with a previously resonant wave, leading to strong resonance broadening. The situation in turbulence is discussed in §3.2.4.

## B. RESONANCE BROADENING IN WEAK TURBULENCE

### B.1. Turbulence Model

In the main text, we considered a resonance broadening model where the underlying turbulence spectrum was purely strong GS turbulence. In this appendix, we discuss an expansion of the model to the case of weak turbulence.

We consider MHD turbulence that is driven isotropically with an outer scale eddy velocity  $v_L < v_A$ . The turbulence at the outer scale is weak in the sense that the linear time scale for wave propagation is shorter than the nonlinear time scale for eddy turnover,  $L_{\parallel}/v_A < L_{\perp}/v_L$ , where isotropy implies that  $L_{\parallel} = L_{\perp} \equiv L$ . This implies that waves live for more than one wave period before they decay. We may express this weak turbulence requirement more generally by noting that the non-linearity parameter  $\chi \equiv v_l l_{\parallel}/v_A l_{\perp} < 1$ , where  $l_{\parallel}$  and  $l_{\perp}$  refer to scales smaller than  $L$ , and  $v_l$  is the turbulent eddy velocity on that scale.

However, weak turbulence cascades only in the perpendicular direction to higher  $k_{\perp}$  (Shebalin et al. 1983; Galtier et al. 2000), while no structure on smaller parallel scales develops. This implies a 1D power spectrum  $E_k \propto k_{\perp}^{-2}$  (Ng & Bhattacharjee 1997). However,  $\chi \propto k_{\perp}^{1/2}$ , so that the non-linearity increases at smaller scales. Eventually, when  $\chi \sim 1$ , the turbulence reaches the strong critically balanced state of GS, and the cascade proceeds to smaller scales at fixed  $\chi$  of order unity. Critical balance refers to the balance of wave and eddy time scales. This implies that most of the turbulent energy is contained in eddies with  $k_{\parallel} \propto k_{\perp}^{2/3}$ , and a 1D power spectrum  $E_k \propto k_{\perp}^{-5/3}$ . The transition between the weak and strong regimes occurs at a wavenumber  $k_{\perp,c} = (2\pi/L)M_A^{-2}$ , where  $M_A = v_L/v_A$  is the Alfvénic Mach number at the outer scale.

More quantitatively, we define the 3D power spectrum as

$$I(\mathbf{k}) = I_w(\mathbf{k}) + I_s(\mathbf{k}), \quad (\text{B1})$$

where the weak and strong contributions to the power spectrum are given respectively by

$$I_w(\mathbf{k}) \equiv A_w k_{\perp}^{-3} \delta(k_{\parallel} - 2\pi/L) g \left[ \frac{k_{\perp}}{k_{\perp,c}} \right], \quad (\text{B2})$$

and

$$I_s(\mathbf{k}) \equiv A_s k_{\perp}^{-10/3} g \left[ \frac{k_{\parallel} L}{2\pi} \left( \frac{k_{\perp}}{k_{\perp,c}} \right)^{-\frac{2}{3}} \right] \left( 1 - g \left[ \frac{k_{\perp}}{k_{\perp,c}} \right] \right), \quad (\text{B3})$$

where  $A_w$  and  $A_s$  are dimensional normalizing coefficients defined below, and  $g(x)$  will be treated as a step function, equal to 1 if  $|x| < 1$ , and 0 otherwise.  $g(x)$  is used in two ways: the first  $g(x)$  in Equation B3 accounts for the fact that power only resides inside the critically balanced cone of wavenumbers, while the other instances model the transition from weak to strong turbulence at  $k_\perp = k_{\perp,c}$ .

We fix the normalizing coefficients  $A_w$  and  $A_s$  by first requiring that the total energy in the turbulence be given by an integral over the power spectrum,

$$\frac{v_L^2}{2} = \frac{1}{(2\pi)^3} \int d^3\mathbf{k} I(\mathbf{k}). \quad (\text{B4})$$

Because there are two coefficients  $A_w$  and  $A_s$ , we require another condition, which is given by the requirement that the 1D weak and strong power spectra must match up at the transition scale:

$$\int dk_\parallel I_w(\mathbf{k}) \Big|_{k_{\perp,c}} = \int dk_\parallel I_s(\mathbf{k}) \Big|_{k_{\perp,c}} \quad (\text{B5})$$

Taken together, these two requirements imply that

$$A_w = 2A_s \left( \frac{2\pi}{L} M_A \right)^{\frac{2}{3}} \quad (\text{B6})$$

and

$$A_s = (2\pi)^2 \frac{v_L^2}{4F} M_A^{-\frac{2}{3}} \left( \frac{2\pi}{L} \right)^{\frac{1}{3}}, \quad (\text{B7})$$

where  $F$  is given by

$$F = (1 - M_A^2) + \frac{3}{2} \left( \frac{M_A}{N} \right)^{\frac{2}{3}} \left[ (NM_A^2)^{\frac{2}{3}} - 1 \right], \quad (\text{B8})$$

and  $N \equiv L/L_{\min}$  is the range of scales in the turbulent cascade. For  $N \gg 1$ ,  $F$  is approximately constant and equal to 1 until  $M_A$  is near unity, and then increases sharply to 3/2 as  $M_A \rightarrow 1$ . Recent work which demonstrates a transition from weak to strong turbulence (Howes et al. 2011b; Verdini & Grappin 2012) supports the basic form of this turbulence model.

## B.2. Resonance Broadening

We use the same resonance broadening model as in the main text (see Equation 5). For weak turbulence, this approach must be modified slightly to reflect the fact that while  $\chi$  is the fractional energy change of a wave in one wave period, the energy change could be randomly positive or negative, and the energy of the wave will diffuse in energy space. Thus we estimate that the actual decoherence time of waves will be typically given by  $\omega_{\text{dec}} = \chi^2 \omega_{\text{lin}}$ .

As before, the exponential resonance function is given by

$$R_{\text{exp}}(\mathbf{k}) = \frac{\gamma \omega_{\text{dec}}}{\gamma^2 \omega_{\text{dec}}^2 + k_\parallel^2 (v_\parallel \pm v_p)^2}, \quad (\text{B9})$$

where  $\omega_{\text{dec}}$  scales differently with  $k_\perp$  in the weak and strong cases. We see that the resonance function is still peaked at  $|v_\parallel| = v_p$ , but becomes a Lorentzian in  $v_\parallel$  rather than a delta-function.

The diffusion coefficient is a sum of the contributions from the weak and strong turbulence components. To calculate the contribution from weak turbulence, we use the weak power spectrum of Equation B2, and a non-linear frequency given by  $\omega_{\text{dec}} = k_\perp v_L^2 / v_A$  to find

$$D_{\parallel,w} = \frac{G'}{16u_+^2} \left\{ \frac{u_+^2}{u_-^2} \ln \left( \frac{M_A^4 + u_-^2}{M_A^4 (u_-^2 + 1)} \right) + \ln \left( \frac{M_A^4 + u_+^2}{M_A^4 (u_+^2 + 1)} \right) \right\} \quad (\text{B10})$$

where

$$G' \equiv \frac{1}{F} \frac{2\pi}{L} \frac{v_\perp^4}{\gamma v_A} M_A^4, \quad (\text{B11})$$

and  $u_\pm = (v_\parallel \pm v_p) / (\gamma v_A)$ .

Beyond the transition to strong turbulence at  $k_{\perp,c}$ , the decorrelation frequency is given by  $\omega_{\text{dec}} = \omega_{\text{nl}} = (2\pi v_A / L) (k_\perp / k_{\perp,c})^{2/3}$ , and the power spectrum is given by Equation B3. In this case we find

$$D_{\parallel,s} = \frac{G'}{8u_+^2} \ln [NM_A^2] \left\{ \left( 1 + \frac{u_+^2}{u_-^2} \right) - \frac{1}{u_+} \left( \frac{u_+^3}{u_-^3} \arctan u_- + \arctan u_+ \right) \right\}, \quad (\text{B12})$$

which is again strongly broadened with an asymptotic form as  $|v_{\parallel}| \gg v_p$  of  $D_{\parallel,s} \propto v_{\parallel}^{-2}$ . For  $M_A \lesssim 0.5$ , the strong turbulence diffusion coefficient in Equation B12 is significantly more broadened than the weak turbulence diffusion coefficient in Equation B10, as we show explicitly in Figure 14 discussed below.

As in the main text, we also examine a *Gaussian decorrelation* model, where we replace the decorrelation term  $\gamma\omega_{\text{dec}}t$  with  $(\gamma\omega_{\text{dec}}t)^2$ . In this case, we find the Gaussian resonance function,

$$R_{\text{gauss}}(\mathbf{k}) = \frac{\sqrt{\pi}}{2\gamma\omega_{\text{dec}}} \exp\left[-\frac{(\omega - k_{\parallel}v_{\parallel})^2}{4\gamma^2\omega_{\text{dec}}^2}\right], \quad (\text{B13})$$

so that the  $\delta$ -function becomes a Gaussian resonance. Now, using Equation 3, we find

$$D_{\parallel,w} = \frac{\sqrt{\pi} G'}{8 u_+^2} \left\{ \frac{u_+^2}{u_-^2} \left( e^{-\frac{u_-^2}{4}} - e^{-\frac{u_-^2}{4M_A^4}} \right) + e^{-\frac{u_+^2}{4}} - e^{-\frac{u_+^2}{4M_A^4}} \right\} \quad (\text{B14})$$

and

$$D_{\parallel,s} \equiv \frac{\sqrt{\pi} G'}{8 u_+^3} \ln [NM_A^2] \times \left\{ -\frac{u_+^3}{u_-^2} e^{-u_-^2/4} - u_+ e^{-u_+^2/4} + \sqrt{\pi} \left[ \frac{u_+^3}{u_-^2} \text{erf}[u_-/2] + \text{erf}[u_+/2] \right] \right\} \quad (\text{B15})$$

where  $\text{erf}(x)$  is the error function. In the  $|v_{\parallel}| \gg v_p$  limit,  $D_{\parallel,w}$  cuts off exponentially, while  $D_{\parallel,s} \propto |v_{\parallel}|^{-3}$ .

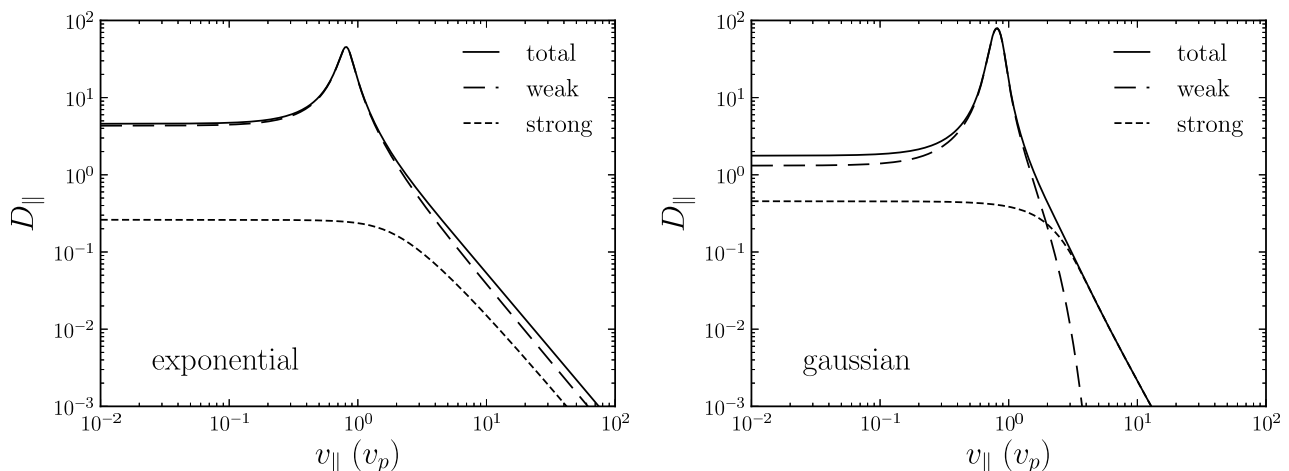


FIG. 14.— Diffusion coefficients (arbitrary normalization) for transit-time damping by slow modes in exponential (left) and Gaussian (right) decorrelation models.  $M_A = v_L/v_A = B_L/B_0 = 0.25$ , and  $v_p \simeq 0.81$ ,  $v_A = \sqrt{2}$ , corresponding to slow modes with  $\beta = 1$ . For this choice of  $M_A$  we see that weak turbulence on the outer scales is the dominant contribution to the velocity diffusion, although the  $|v_{\parallel}|^{-3}$  tail from strong turbulence is important at high  $v_{\parallel}$  in the Gaussian model.

In Figure 14 we plot representative examples of  $D_{\parallel}$  for exponential and Gaussian decorrelation models, with the same arbitrary normalization. We choose  $\gamma = 1$  and  $\gamma = 0.5$  for the exponential and Gaussian models respectively, as in the main text. The diffusion coefficients display a sharp peak around the resonant phase velocity. In Figure 8 in the main text we plotted the corresponding diffusion coefficients for a run with even lower amplitude turbulence ( $M_A \simeq 0.11$ ), for which this model would predict a yet sharper resonance. No clear peak could be seen. We interpret that this is the result of additional phase-decorrelation broadening due to finite-amplitude turbulence (§3.2.4), which we do not quantitatively model.

### C. TURBULENCE POWER SPECTRA

In Figure 15, we show the 2D power spectra of fully saturated turbulence for two different simulations, one with  $t_{\text{corr}} = 0.1 L/c_s$  (left panel) and one with  $t_{\text{corr}} = 1.5 L/c_s$  right panel. In all other respects the simulations are identical and have the fiducial parameters of Table 1, with an eddy turnover time of approximately  $t_{\text{eddy}} \sim (L/2)/v_L \sim 1.5 L/c_s$ .

The simulation with the longer correlation time develops significant power on low  $k_{\parallel}$ , which are not driven by our turbulence driving routine, while the simulation with the shorter correlation time does not develop power on similar scales. We believe that this is due to frequency matching of waves with the frequency content of the Ornstein-Uhlenbeck driving routine, so that modes with  $k_{\parallel}v_A \sim t_{\text{corr}}^{-1}$  naturally develop power despite not being actively driven in k-space.

We also note that the longer- $t_{\text{corr}}$  simulation has a one-dimensional power spectrum consistent with  $P \propto k^{-5/3}$ , while the simulation with the shorter correlation time has a somewhat steeper power spectrum, possibly consistent with  $P \propto k^{-2}$  (though our lack of inertial range does not allow us to make this statement with any confidence). This

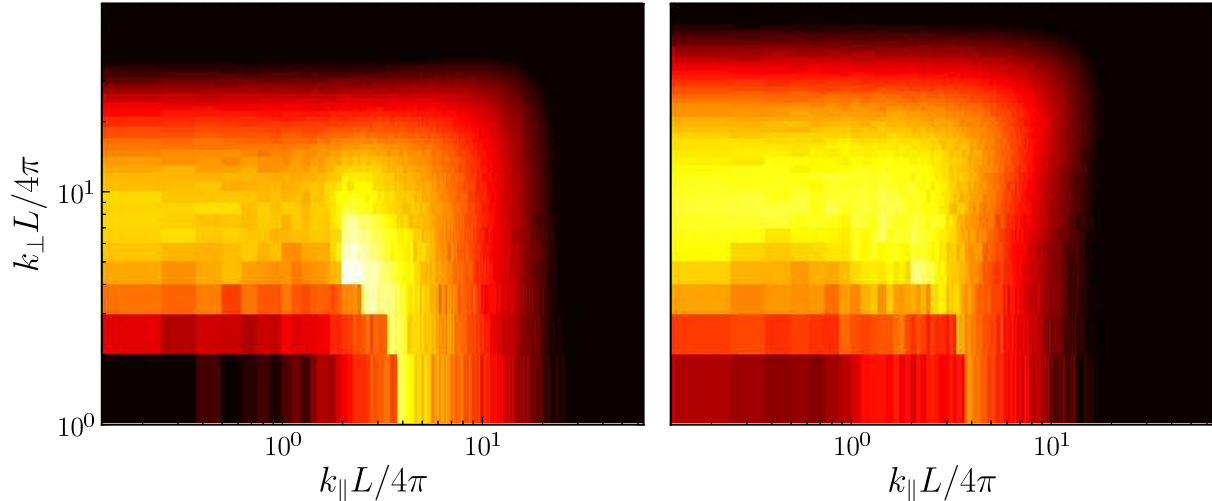


FIG. 15.— Two-dimensional plots of  $P(\mathbf{k})k^3$  in  $\{k_{\parallel}, k_{\perp}\}$ -space for saturated turbulence with  $t_{\text{corr}} = 0.1 L/c_s$  (left panel) and  $t_{\text{corr}} = 1.5 L/c_s$  (right). All other parameters are for our fiducial case, given in Table 1. Color normalization is logarithmic and identical, with white and yellow corresponding to the highest values, and red and black corresponding to the lowest values. Despite the fact that modes with  $k_{\parallel} < 4\pi/L$  are not driven, frequency-matching of long-wavelength Alfvén waves with the long  $t_{\text{corr}}$  leads to the development of power in low- $k_{\parallel}$  modes. In the run with a shorter correlation time, power is much more concentrated in the driven volume of  $k$ -space. See discussion in Appendix C.

seems consistent with the idea that the extra power at low  $k_{\parallel}$  in the run with the longer correlation time provides anisotropy that can actually lead to critical balance on the outer scales. In other words,  $\chi \sim k_{\perp} v_L / k_{\parallel} v_A \sim 1$  because  $k_{\parallel} / k_{\perp} \sim v_L / v_A$  as a result of frequency matching. We do not attempt to explicitly model this behavior in the main body of the paper, however, choosing instead to focus on the simpler and more generic case of isotropic strong turbulence. Furthermore, the test particle diffusion coefficients do not demonstrate any obvious peakiness for the shorter  $t_{\text{corr}}$  case, suggesting that despite the apparent weaker turbulence, the diffusion coefficients are not well-described by the turbulence model we discuss in Appendix B. We believe that this is a result of the phase-decorrelation broadening discussed in §3.2.4.